NASA Technical Memorandum 101985
ICOMP-89-12

Multiwave Interactions in Turbulent Jets

Reda R. Mankbadi
Institute for Computational Mechanics in Propulsion
Lewis Research Center
Cleveland, Ohio

September 1989

NASA

INSTITUTE FOR COMPUTATIONAL MECHANICS IN PROPULSION
NASA LEWIS RESEARCH CENTER
ICOMP
CASE WESTERN RESERVE UNIVERSITY

MULTIWAVE INTERACTIONS IN TURBULENT JETS

Reda R. Mankbadi*
Institute for Computational Mechanics in Propulsion
Lewis Research Center
Cleveland, Ohio 44135

SUMMARY

Nonlinear wave-wave interactions in turbulent jets were investigated based on the integrated energy of each scale of motion in a cross section of the jet. The analysis indicates that two frequency components in the axisymmetric mode can interact with other background frequencies in the axisymmetric mode, thereby amplifying an enormous number of other frequencies. Two frequency components in a single helical mode cannot, by themselves, amplify other frequency components. But combinations of frequency components of helical and axisymmetric modes can amplify other frequencies in other helical modes. The present computations produce several features consistent with experimental observations such as (1) dependency of the interactions on the initial phase differences, (2) enhancement of the momentum thickness under multifrequency forcing, and (3) an increase in background turbulence under forcing. In a multifrequency-excited jet, mixing enhancement was found to be a result of the turbulence enhancement rather than simply the amplification of forced wave components. The excitation waves pump energy from the mean flow to the turbulence, thus enhancing the latter. The high-frequency waves enhance the turbulence close to the jet exit, but the low-frequency waves are most effective further downstream.

INTRODUCTION

The study of artificially excited shear flows may provide insight into the physical mechanisms governing the onset and evolution of turbulence in shear flows. Such studies can provide a guide for formulating new predictive turbulence models and for controlling lift and drag as well as turbulent mixing and transport. Motivated by understanding laminar-turbulent transitions, Miksad (refs. 1 and 2) excited a shear layer with two frequencies of comparable growth rates. The two imposed waves interacted nonlinearly, generating the sum and difference modes and the harmonics and subharmonics of the forcing frequencies. Some of these components were found to grow and interact with others, generating additional components. Finally an enormous number of waves were generated, leading to a complete transition to fully turbulent flow. Because of the complexity of this experiment, most later experiments concentrated on single-frequency excitation.

Single-frequency excitation has now been studied by many researchers: for example, Binder and Favre-Marinet (refs. 3 and 4), Ho and Huang (ref. 5), Mankbadi and Liu (ref. 6), Mankbadi (ref. 7), Winant and Browand (ref. 8) and Zaman and Hussain (ref. 9), to mention only a few. An excellent review for the work in this area is given in an article by Ho and Huerre (ref. 10). In

---

*Work funded under Space Act Agreement C99066G.

general, these investigations indicate that the shear-layer spreading rate can be controlled effectively by forcing.

The possibility of using two-frequency forcing to extend the range over which the flow can be controlled has been explored by Wygnanski and Petersen (ref. 11), Raman and Rice (ref. 12), and Bradley (ref. 13). These observations indicate that forcing at two frequencies makes the shear layer grow faster than forcing at either frequency alone at the same forcing level. Thus, combined-mode forcing is not only significant to the fundamental understanding of the laminar-turbulent transition, but is also significant to the technologically important problem of mixing and turbulence control. The importance of two-frequency forcing has motivated several studies to understand the wave-wave interactions in two-frequency excitations. Numerical simulations of temporal instability in a shear layer (refs. 14 and 15) and of spatial stability in a laminar axisymmetric shear layer (ref. 16) show that the wave-wave interaction process is highly dependent on the phase alignment. This was confirmed experimentally by Zhang, Ho, and Monkewitz (ref. 17) for the shear layer. For a round jet, Arbey and Ffowcs-Williams (ref. 18) observed a phase-dependent suppression of the first subharmonic in the pressure spectrum when the jet was excited at the natural frequency and its first subharmonic. Furthermore, the experimental observations of Raman and Rice (ref. 12) show that for high levels of excitations, the phase development of the stability waves is a highly nonlinear process.

This report presents formulations for multifrequency interactions in the axisymmetric or azimuthal modes. These wave-wave interactions are coupled with their interactions with the fine-grained background turbulence. The purpose is to provide a model for a multifrequency excited jet and to increase the understanding of the later stages of the laminar-turbulence transition. High-amplitude excitations are emphasized so that the maximum effect on jet mixing can be observed. The nonlinear development of the wave amplitudes are coupled with the nonlinear development of the phase angles, which Raman and Rice's (ref. 12) observations indicate to be significant in high-amplitude excitations.

ANALYSIS

The problem considered here is that of a turbulent jet issuing from a nozzle of radius R, the Mach number is small, and the compressibility effects are negligible. The coordinate system is (x,r,ϕ) where x is the streamwise direction, r is the radial direction, and ϕ is the azimuthal angle. The corresponding velocity components are u, v, and w. Velocities are normalized by the jet exit velocity U_e, distances by the nozzle radius R, and the pressure by ρU_e^2, where ρ is the fluid density. The time t is normalized by R/U_e.

The fluid motion is split into three kinds of motion: a time-averaged motion $\bar{U}_i(\underline{x})$; a periodic, organized, large-scale wavelike structure $\tilde{u}_i(\underline{x},t)$; and a background, fine-scale random turbulence $u_i'(\underline{x},r)$. Thus,

$$u_i(\underline{x},t) = \bar{U}_i(\underline{x}) + \tilde{u}_i(\underline{x},t) + u_i'(\underline{x},r) \tag{1}$$

and the pressure, P, is similarly split. An overbar denotes the usual time average of the flow quantity. The periodic, wavelike component is taken to be represented by a finite number of frequency and azimuthal components. Thus,

$$\tilde{u}(\underline{x},t) = \sum_m \sum_n u_{mn}(\underline{x},r)\exp(-i\omega_m t + iN_n\phi) + cc \tag{2}$$

where cc or * denotes the complex conjugate. We consider here the interactions among these frequency and azimuthal components along with their interactions with the mean flow and the background turbulence. These interactions are viewed within the framework of the energy exchanges among the different scales of motion. To derive the governing equations for each flow component, the usual phase-averaging technique (refs. 19 and 20) is extended to apply to a given azimuthal number in addition to the usual definition with respect to the frequency. Thus,

$$\left\langle \sum_m \sum_n g_{mn}(\underline{x},r)\exp(-\omega_n t + iN_n\phi) \right\rangle = g_{mn}(x,r)\exp(-\omega_m t + iN_n\phi)$$

The mean flow momentum equation is derived by substituting the decomposition of equation (1) into the full, unsteady Navier-Stokes equations for incompressible flow in cylindrical coordinates and by taking the time average. The mean flow energy equation is obtained by multiplying each component of the mean flow momentum equation by the corresponding velocity and adding. The resulting mean flow kinetic energy equation is

$$\left.\begin{aligned} \bar{U}_j \frac{\partial \bar{U}_i^2/2}{\partial x_j} - \frac{1}{r}\left[v\left(\bar{w}^2 + \overline{\tilde{w}^2} + \overline{w'^2}\right) - \bar{w}\left(\overline{wv} + \overline{\tilde{w}\tilde{v}} + \overline{w'v'}\right)\right] \\ = -\left[-\left(\tilde{u}_i\tilde{u}_1 + \overline{u_i'u_1'}\right)\frac{\partial \bar{U}_i}{\partial x_j}\right] - \frac{\partial}{\partial x_j^*}\left[\bar{U}_i\left(\tilde{u}_i\tilde{u}_j + \overline{u_i'u_j'}\right)\right] - \frac{\partial}{\partial x_i^*}\left(\overline{pU_i}\right) \\ + \frac{1}{Re}\left[\bar{U}_i \nabla^2 \bar{U}_i - \frac{\bar{V}}{r^2}\left(\bar{V} + 2\frac{\partial \bar{W}}{\partial \phi}\right) - \frac{\bar{W}}{r^2}\left(\bar{W} - 2\frac{\partial \bar{V}}{\partial \phi}\right)\right] \end{aligned}\right\} \tag{3}$$

where

$$\frac{\partial}{\partial x_j^*} = \left(\frac{\partial}{\partial r}, \frac{1}{r}\frac{\partial}{\partial r}(r), \frac{1}{r}\frac{\partial}{\partial \phi}\right)$$

The kinetic energy equation of the turbulent motion is derived as follows. The time-averaged momentum equation is subtracted from the full momentum equation. Each component of the momentum equation is multiplied by the corresponding velocity component u_i', and the three components are added and time averaged. Triple correlations that contain an odd number of random components are zero; those containing an even number of random components are not zero. The resulting kinetic energy equation of the turbulence is

$$
\left.
\begin{aligned}
&\overline{U_j}\,\frac{\partial \bar{q}}{\partial x_j} - \frac{1}{r}\left(-\bar{V}\,\overline{w'^2} + \bar{W}\,\overline{w'v'} - \overline{\tilde{V}w'w'} + \overline{\tilde{W}w'v'}\right) \\
&\qquad = -\overline{u_i'u_j'}\,\frac{\partial \overline{U_i}}{\partial x_j} + \overline{\left(-u_i'u_j' - \overline{u_i'u_j'}\right)\frac{\partial \tilde{u}_i}{\partial x_j}} - \frac{\partial}{\partial x_j}\left(\overline{u_j'(P' + q)} + \overline{\tilde{u}_j q}\right) \\
&\qquad\quad + \frac{1}{Re}\left[\overline{u_i'\,\nabla^2 u_i'} - \frac{1}{r^2}\left(\overline{v'^2} - 2\overline{V'\,\frac{\partial w'}{\partial \phi}}\right) - \frac{1}{r^2}\left(\overline{w'^2} - 2\overline{w'\,\frac{\partial V'}{\partial \phi}}\right)\right]
\end{aligned}
\right\} \qquad (4)
$$

where

$$
q = \sum \frac{1}{2}\,u_i'^2
$$

The energy equation for a wave component of frequency ω_m and azimuthal number N_n is obtained as follows. The full momentum equation is first phase averaged with respect to the frequency under consideration, and the time-averaged equation is subtracted from the phase-averaged one. The resulting equation contains all the azimuthal components of frequency ω_m. To separate the azimuthal component, we multiply the ω–momentum equation by $\exp(-iN_n\phi)$ and integrate it over ϕ. This produces a momentum equation for the mn-frequency-azimuthal component. This equation is multiplied by the corresponding velocity $\tilde{u}_{i,mn}$ to yield the kinetic energy equation for the mn-wave component:

$$
\begin{aligned}
&\overline{U_j}\,\frac{\partial \overline{Q_{mn}}}{\partial x_j} - \frac{1}{r}\left(-\overline{V}\langle\tilde{w}^2\rangle_{mn} + \overline{W}\langle\tilde{w}\tilde{v}\rangle_{mn}\right) \\
&\quad = -\overline{\tilde{u}_{i,mn}\tilde{u}_{j,mn}}\,\frac{\partial \overline{U_i}}{\partial x_j} - \left(-\overline{\tilde{r}_{ij,mn}\,\frac{\partial \tilde{u}_{i,mn}}{\partial x_j}} - \overline{\tilde{v}_{mn}\tilde{r}_{\phi\phi,mn}} + \overline{\tilde{w}_{mn}\tilde{r}_{r\phi,mn}}\right) \\
&\quad - \left(-\overline{\langle\tilde{u}_i\tilde{u}_j\rangle_{mn}\,\frac{\partial \tilde{u}_{i,mn}}{\partial x_j}} - \overline{\tilde{v}_{mn}\langle\tilde{w}^2\rangle_{mn}} - \overline{\tilde{w}_{mn}\langle\tilde{w}\tilde{v}\rangle_{mn}}\right) \\
&\quad - \frac{\partial}{\partial x_j^*}\left(\overline{\tilde{u}_{i,mn}\tilde{r}_{ij,mn}} + \overline{\tilde{u}_{j,mn}\tilde{P}_{mn}} + \overline{\tilde{u}_{i,mn}\langle\tilde{u}_i\tilde{u}_j\rangle_{mn}}\right) \\
&\quad + \frac{1}{Re}\left[\overline{\tilde{u}_{i,mn}\nabla^2\tilde{u}_{i,mn}} - \frac{1}{r^2}\left(\overline{\langle\tilde{v}^2\rangle_{mn} + \langle\tilde{w}^2\rangle_{mn} - 2\,\frac{\partial}{\partial\phi}\langle\tilde{v}\tilde{w}\rangle_{mn}}\right)\right]
\end{aligned}
\qquad (5)
$$

where

$$\phi = \sum \frac{1}{2}\,\tilde{u}_i^2$$

and

$$\tilde{r}_{ij,mn} = \langle u_i' u_j'\rangle_{mn} - \overline{u_i' u_j'}$$

The dynamic equation for the wave-induced stresses $\tilde{r}_{ij,mn}$ is derived as follows. The u_i'-momentum equation is multiplied by u_j', and vice versa, to form the equations for the instantaneous Reynolds stresses. By taking the difference between the phase average and time average of the instantaneous Reynolds stresses, the following equation for $\tilde{r}_{ij}$ is obtained:

$$\frac{D\tilde{r}_{ij,mn}}{Dt} + \left\langle \tilde{u}_k \frac{\partial u_i' u_j'}{\partial x_j} \right\rangle_{mn} - \tilde{u}_k \frac{\partial \overline{u_i' u_j'}}{\partial x_j} + \tilde{r}_{jk,mn} \frac{\partial \overline{U_i}}{\partial x_k} + \langle r_{ik} \rangle_{mn} \frac{\partial \overline{U_j}}{\partial x_k} + \langle X_{ij} \rangle_{mn}$$

$$= -\left(\left\langle u_j' u_k' \frac{\partial \tilde{u}_i}{\partial x_k} \right\rangle_{mn} - \overline{u_j' u_k'} \frac{\partial \tilde{u}_i}{\partial x_k} \right) - \left(\left\langle u_i' u_k' \frac{\partial \tilde{u}_j}{\partial x_k} \right\rangle_{mn} - \overline{u_i' u_k'} \frac{\partial \tilde{u}_j}{\partial x_k} \right)$$

$$- \left(\left\langle u_i' \frac{\partial P'}{\partial x_j} \right\rangle_{mn} - \overline{u_i' \frac{\partial P'}{\partial x_j}} + \left\langle u_j' \frac{\partial P'}{\partial x_j} \right\rangle_{mn} - \overline{u_j' \frac{\partial P'}{\partial x_j}} \right)$$

$$+ \frac{\partial}{\partial x_k^*} \left(\overline{u_i' u_j' u_k'} - \langle u_i' u_j' u_k' \rangle_{mn} \right)$$

$$+ \frac{1}{Re} \left(\nabla^2 \langle \tilde{r}_{ij} \rangle_{mn} - 2 \left\langle \frac{\partial u_i'}{\partial x_k} \frac{\partial u_j'}{\partial x_k} \right\rangle_{mn} + 2 \overline{\frac{\partial u_i'}{\partial x_k} \frac{\partial u_j'}{\partial x_k}} - \frac{Y_{ij}}{r^2} \right) \qquad (6a)$$

where

$$\begin{bmatrix} X_{xx} \\ X_{rr} \\ X_{\phi\phi} \\ X_{xr} \\ X_{x\phi} \\ X_{r\phi} \end{bmatrix} = \frac{1}{r} \begin{bmatrix} 0 \\ -2\left(\overline{2W}\tilde{r}_{\phi r} + 2\tilde{w}\langle w'v' \rangle - 2\overline{\tilde{w}w'v'} + \langle w'^2 v' \rangle - \overline{w'^2 v'} \right) \\ 2\left(\overline{V}\tilde{r}_{\phi\phi} + \tilde{v}\langle w'^2 \rangle - \overline{\tilde{v}w'^2} + \tilde{w}\langle v'w' \rangle - \overline{\tilde{w}v'w'} + \overline{W}\tilde{r}_{\phi r} + \langle v'w'^2 \rangle - \overline{v'w'^2} \right) \\ -\overline{2W}\tilde{r}_{x\phi} + 2\tilde{w}\langle w'u' \rangle - 2\overline{\tilde{w}w'u'} + \langle w'^2 u' \rangle - \overline{w'^2 u'} \\ \overline{V}\tilde{r}_{x\phi} + \overline{W}\tilde{r}_{xr} + \tilde{v}\langle w'u' \rangle - \overline{\tilde{v}w'u'} + \tilde{w}\langle v'u' \rangle - \overline{\tilde{w}v'u'} + \langle u'v'w' \rangle - \overline{u'v'w'} \\ -\left(\overline{2W}\tilde{r}_{\phi\phi} + 2\tilde{w}\langle w'^2 \rangle - \overline{2\tilde{w}w'^2} + \langle w'^3 \rangle - \overline{w'^3} \right) + \overline{V}\tilde{r}_{\phi r} + \tilde{v}\langle w'v' \rangle - \overline{\tilde{v}w'v'} \\ + \tilde{w}\langle v'^2 \rangle - \overline{\tilde{w}v'^2} + W\tilde{r}_{rr} + \langle v'^2 w' \rangle - \overline{v'^2 w'} \end{bmatrix}$$

(6b)

and

$$\begin{bmatrix} Y_{xx} \\ Y_{rr} \\ Y_{\phi\phi} \\ Y_{xr} \\ Y_{x\phi} \\ Y_{r\phi} \end{bmatrix} = \begin{bmatrix} 0 \\ 2\left(\tilde{r}_{rr} + 2\left\langle v' \frac{\partial w'}{\partial \phi}\right\rangle - \overline{2v' \frac{\partial w'}{\partial \phi}}\right) \\ 2\left(\tilde{r}_{\phi\phi} - 2\left\langle w' \frac{\partial v'}{\partial \phi}\right\rangle + \overline{2w' \frac{\partial v'}{\partial \phi}}\right) \\ \tilde{r}_{xr} + 2\left\langle u' \frac{\partial w'}{\partial \phi}\right\rangle - \overline{2u' \frac{\partial w'}{\partial \phi}} \\ \tilde{r}_{x\phi} - 2\left\langle u' \frac{\partial v'}{\partial \phi}\right\rangle + \overline{2u' \frac{\partial v'}{\partial \phi}} \\ 2\tilde{r}_{\phi r} + 2\left\langle w' \frac{\partial w'}{\partial \phi}\right\rangle - \overline{2w' \frac{\partial w'}{\partial \phi}} \; 2\left\langle v' \frac{\partial v'}{\partial \phi}\right\rangle + \overline{2v' \frac{\partial v'}{\partial \phi}} \end{bmatrix} \tag{6c}$$

Integral Energy Equations

The integral energy equation of the mean flow is obtained by applying the boundary-layer-type approximations to the mean quantities. These approximations imply that $\partial(\bar{\ })/\partial x \ll \partial(\bar{\ })/\partial r$, $\bar{V} \ll \bar{U}$, and that the mean flow is axisymmetric with $\bar{W} = 0$. These approximations are applied to equation (3), viscous terms are neglected, and the equation is integrated over r and ϕ. The resulting mean flow energy equation is given by

$$\frac{1}{2}\frac{d}{dx}\int_0^\infty \bar{U}^3 r\, dr = -\int_0^\infty -\overline{\tilde{u}\tilde{v}}\,\frac{\partial \bar{U}}{\partial r}\, r\, dr - \int_0^\infty -\overline{u'v'}\,\frac{\partial \bar{U}}{\partial r}\, r\, dr \tag{7a}$$

As it will be shown later on, $\overline{\tilde{u}\tilde{v}}$, in general, contains azimuthal terms that can distort the axisymmetry of the mean flow. These azimuthal terms vanish upon integration over ϕ. Therefore the integration over ϕ was necessary to be consistent with the assumed axisymmetry of the mean flow. Equation (7a) therefore represents the mean flow energy in a transverse section of the jet.

Equation (7a) can be written as

$$\frac{d\theta}{dx}\frac{1}{2}\frac{d}{d\theta}\int_0^\infty \bar{U}^3\, r\, dr = -MW - MT \tag{7b}$$

where θ is the momentum thickness and MW and MT are the first and second integrals in the right side of equation (7a), respectively. Equation (7) states that the growth of the momentum thickness (the drain of the mean flow

energy) is governed by the mean flow production of the wave components MW and by the mean flow production of the turbulence MT.

The integral energy equation for the random turbulence is obtained by applying boundary-layer-type approximations to the mean quantities and by handling the viscous dissipation terms in the usual manner. After integrating over r and ϕ, the turbulence kinetic energy equation reduces to

$$\frac{d}{dx}\int_0^\infty \bar{q}\,\bar{U}\,r\,dr = \int_0^\infty -\overline{u'v'}\,\frac{\partial U}{\partial r}\,r\,dr + \int_0^\infty \left(\overline{\tilde{r}_{ij}\,\frac{\partial u_i}{\partial x_j}} - \frac{\tilde{v}}{r}\,\tilde{r}_{\phi\phi} + \frac{\tilde{w}}{r}\,\tilde{r}_{r\phi}\right) r\,dr$$

$$- \frac{1}{Re}\int_0^\infty \overline{\frac{\partial u_i'}{\partial x_k}\,\frac{\partial u_i'}{\partial x_k}}\,r\,dr \qquad (8a)$$

This equation can be written as

$$\frac{d}{dx}\int_0^\infty \bar{q}\,\bar{U}\,r\,dr = MT + WT - dis \qquad (8b)$$

Equations (8a) and (8b) state that the development of the turbulence energy is governed by its production by the mean flow MT, the energy transfer from the wave WT, and the turbulence dissipation dis.

The integral energy equation for the mn-wave component is obtained from the full energy equation (5) in the same manner:

$$\left.\begin{aligned}\frac{d}{dx}\int_0^\infty \bar{U}\,\overline{Q_{mn}}\,r\,dr &= \int_0^\infty -\overline{\tilde{u}_{mn}\tilde{v}_{mn}}\,\frac{\partial \bar{U}}{\partial r}\,r\,dr - \int_0^\infty \overline{\Phi_{mn}}\,r\,dr \\ &+ \int_0^\infty \left(\overline{\langle \tilde{u}_i\tilde{u}_j\rangle_{mn}\,\frac{\partial \tilde{u}_{i,mn}}{\partial x_j}} + \frac{1}{r}\,\tilde{v}_{mn}\langle\tilde{w}^2\rangle_{mn} - \tilde{w}_{mn}\langle\tilde{w}\tilde{v}\rangle_{mn}\right) r\,dr\end{aligned}\right\} \qquad (9a)$$

where

$$-\bar{\Phi} = \overline{\tilde{r}_{ij,nn}\,\frac{\partial \tilde{u}_{i,mn}}{\partial x_j}} + \frac{1}{r}\,\overline{\tilde{v}_{mn}\tilde{r}_{\phi\phi,mn}} - \overline{\frac{\tilde{w}_{mn}}{r}\,\tilde{r}_{\phi r,mn}}$$

This system of equations can be written in the form

$$\frac{d}{dx}\int_0^\infty \bar{U}\,\bar{Q}_{mn}\,r\,dr = MW_{mn} - WT_{mn} + WW_{mn} \tag{9b}$$

which states that the development of the wave energy is governed by the mean flow production of this particular wave MW_{mn}, by the energy transfer between this wave and the turbulence WT_{mn}, and by the interactions between this wave and other existing waves WW_{mn}.

Mode Decomposition and Interactions

The integral energy equations (eqs. (7) to (9)) are the basis for the present analysis. In these equations, terms representing wave interactions are given in their most general forms, which are applicable to any number of frequency and azimuthal components. The decomposition of these terms for a given number of wave components yields

$$\tilde{u}_i = \sum_{m,n} \tilde{u}_{i,mn}\exp(-i\omega_m t + iN_n\phi) + cc$$

In the mean flow energy equation (7), the production of all waves is given by

$$MW = -\int_0^\infty \overline{\tilde{u}\tilde{v}}\,\frac{\partial \bar{U}}{\partial r}\,r\,dr \tag{10}$$

The waves' Reynolds stress $\overline{\tilde{u}\tilde{v}}$ can, in general, be written as

$$\overline{\tilde{u}\tilde{v}} = \sum_{m,n}\left(u_{mn}v^*_{mn} + cc\right) + \sum_{\substack{m,k,\ell \\ k\neq\ell}}\left\{u_{mk}v^*_{m\ell}\exp\left[i(N_k - N_\ell)\phi\right] + cc\right\} \tag{11}$$

The first summation is over the product uv^* of the same wave. These terms are axisymmetric irrespective of their azimuthal number. The second summation over the product uv^* is produced by the waves of the same frequency but different azimuthal numbers. These terms are not axisymmetric and therefore destroy the symmetry of the mean flow. Note that these terms exist only if there is more than one azimuthal component of the same frequency. Thus, this is consistent with Cohen and Wygnanski's (ref. 21) conclusion that single mode excitation cannot destroy the axisymmetry of the mean flow. The azimuthal terms appearing in equation (11) vanish when integrated over ϕ. Therefore these terms redistribute the mean flow energy in the azimuthal direction but do not contribute to the total energy integrated over ϕ. Since the mean flow energy from equation (10) is integrated over ϕ, these nonaxisymmetric terms vanish and the mean flow production of the wave can be written as

$$MW = \sum_{m,n} MW_{mn} \tag{12}$$

with

$$MW_{mn} = \int_0^\infty u_{mn} v^*_{mn} \frac{\partial \bar{U}}{\partial r} \, r \, dr + cc$$

Thus, the mean flow productions of the waves are given by the linear superposition of the individual mean flow productions of each wave.

In the turbulence energy equation (8), the energy exchange between the waves and the turbulence WT is given by

$$WT = \int_0^\infty \left(\overline{\tilde{r}_{ij} \frac{\partial \tilde{u}_i}{\partial x_j}} - \overline{\frac{\tilde{v}}{r} \tilde{r}_{\phi\phi}} + \overline{\frac{\tilde{w}}{r} \tilde{r}_{r\phi}} \right) r \, dr \tag{13}$$

where the wave-induced stresses $\tilde{r}_{ij} = \langle u'_i u'_j \rangle - \overline{u'_i u'_j}$. Now let us decompose $\tilde{r}$ in a manner similar to $\tilde{u}$: that is,

$$\tilde{r}(x,r,\phi,t) = \sum_{m,n} \tilde{r}_{mn}(x,r) \exp(-i\omega_m t + iN_n \phi) + cc \tag{14}$$

Thus, $\tilde{r}\tilde{u}$ are generally given by

$$\overline{\tilde{r}\tilde{u}} = \sum_{m,n} \left(r_{mn} u^*_{mn} + cc \right) + \sum_{\substack{m,k,\ell \\ k \neq \ell}} \left\{ r_{m\ell} u^*_{mk} \exp\left[i(N_k - N_\ell)\phi \right] + cc \right\} \tag{15}$$

The first summation is over the product produced by the same wave. The second summation is over the product produced by two waves of the same frequency and different azimuthal numbers. This second summation vanishes upon integration over ϕ. Thus, with the energy defined as integrated over ϕ, we can write

$$WT = \sum_{m,n} WT_{mn}$$

with

$$WT_{mn} = \int_0^\infty \left(\overline{r_{ij,mn} \frac{\partial \tilde{u}_{i,mn}}{\partial x_j}} - \overline{\frac{\tilde{v}_{mn}}{r} \tilde{r}_{\phi\phi,mn}} + \overline{\frac{\tilde{w}_{mn}}{r} \tilde{r}_{r\phi,mn}} \right] r \, dr \tag{16}$$

Therefore, the turbulence energy exchange with the waves is given by the sum of the energy exchanges between the turbulence and each individual wave.

Next, we consider the wave-wave interactions appearing in equation (9): namely,

$$WW_{mn} = \int_0^\infty \overline{\left(\langle \tilde{u}_i \tilde{u}_j \rangle_{mn} \frac{\partial \tilde{u}_{i,mn}}{\partial x_j} + \frac{\tilde{v}_{mn}}{r} \langle \tilde{w}^2 \rangle_{mn} - \frac{\tilde{w}_{mn}}{r} \langle \tilde{w}\tilde{v} \rangle_{mn} \right) r} \, dr \tag{17}$$

Because of the time averaging and the azimuthal integration, these terms are generally zero unless ω and N simultaneously satisfy one of the following sets of conditions:

$$\left.\begin{aligned} &\omega_m = \omega_k + \omega_\ell \quad \text{and} \quad N_n = N_k + N_\ell \\ \text{or} \\ &\omega_m = \omega_k - \omega_\ell \quad \text{and} \quad N_n = N_k - N_\ell \end{aligned}\right\} \tag{18}$$

These are the same relations given by Cohen and Wygnanski (ref. 21). Unfortunately, this is not quite a restrictive condition because if one starts with only two frequency components, they can amplify other frequency components that satisfy the conditions of equation (18). If the process is repeated, an enormous number of frequency components can be amplified. The present analysis is applicable to an unlimited number of components. However, for clarity we present only the wave-wave interactions for a limited number of wave components. We consider six wave components: three axisymmetric frequency components and three first-helical frequency components. The frequencies of the helical components match those of the axisymmetric components. These initial wave components can interact with each other to generate an enormous number of other frequency and azimuthal components. However, only the interactions among these initial components are considered. Thus, we force other frequency and azimuthal components to be identically zero.

The frequencies are chosen to satisfy the harmonic relations: that is

$$\omega_m = (2)^{m-1}\omega \tag{19}$$

with $m = 1,2,3$. Thus, each two consecutive frequencies are related to each other by subharmonic-fundamental relations. The lower frequency denotes that of the subharmonic, and the higher denotes that of the fundamental.

The conditions given by equation (18) on the frequency and azimuthal number limit the number of nonzero wave-wave interactions. The wave-wave interactions can be classified into three groups: (1) interactions among the axisymmetric waves, (2) interactions among the helical waves, and (3) mixed interactions between the axisymmetric and the helical waves. The general forms of these interactions will be discussed. The interactions among the axisymmetric waves can be manipulated to be in the form of subharmonic-induced stresses multiplied by fundamental-induced strains. The interactions between the first-helical and the axisymmetric components are formed by two subharmonic frequency components of different azimuthal numbers interacting with the first-helical

fundamental component. The interactions among the helical modes produce non-axisymmetric terms that vanish upon integrating over ϕ. Thus, with the energy defined as that integrated over ϕ, the integrated interactions among the helical modes are identically zero. This is an interesting result since it indicates that, unlike the axisymmetric modes, two first-helical frequency components cannot generate other frequency components. The energy exchanges among the several scales of motion are represented schematically in figure 1. The wave-wave interactions for the six components considered are given by the following equations:

For the axisymmetric ω-component,

$$WW_{10} = -W_{10,10,20} + W_{21,11,10}$$

For the axisymmetric 2ω-component,

$$WW_{20} = W_{10,10,20} - W_{20,20,30} + W_{31,21,20}$$

For the axisymmetric 4ω-component,

$$WW_{30} = W_{20,20,30}$$

For the first-helical ω-component,

$$WW_{11} = -W_{10,11,21} - W_{21,11,10}$$

For the first-helical 2ω-component,

$$WW_{21} = W_{10,11,21} - W_{20,21,31} - W_{31,21,20}$$

For the first-helical 4ω-component,

$$WW_{31} = W_{20,21,31}$$

(20)

where

$$w_{ij,k\ell,mn} = \int_0^{\infty} \left[\overline{\tilde{u}_{ij}\tilde{u}_{k\ell}\frac{\partial \tilde{u}_{mn}}{\partial x}} + \overline{\tilde{v}_{ij}\tilde{u}_{k\ell}\frac{\partial \tilde{v}_{mn}}{\partial x}} + \overline{\tilde{w}_{ij}\tilde{u}_{k\ell}\frac{\partial \tilde{w}_{mn}}{\partial x}} \right.$$

$$+ \overline{\tilde{u}_{ij}\tilde{v}_{k\ell}\frac{\partial \tilde{u}_{mn}}{\partial r}} + \overline{\tilde{v}_{ij}\tilde{v}_{k\ell}\frac{\partial \tilde{v}_{mn}}{\partial r}} + \overline{\tilde{w}_{ij}\tilde{v}_{k\ell}\frac{\partial \tilde{w}_{mn}}{\partial r}}$$

$$+ \frac{1}{r}\left(\overline{\tilde{u}_{ij}\tilde{w}_{k\ell}\frac{\partial \tilde{u}_{mn}}{\partial \phi}} + \overline{\tilde{v}_{ij}\tilde{w}_{k\ell}\frac{\partial \tilde{v}_{mn}}{\partial \phi}} + \overline{\tilde{w}_{ij}\tilde{w}_{k\ell}\frac{\partial \tilde{w}_{mn}}{\partial \phi}} \right)$$

$$\left. + \frac{1}{r}\left(\overline{\tilde{w}_{ij}\tilde{w}_{k\ell}\tilde{v}_{mn}} - \overline{\tilde{v}_{ij}\tilde{w}_{k\ell}\tilde{w}_{mn}} \right) \right] r\, dr \qquad (21)$$

Closure Models

The integral energy equations are used to obtain a set of ordinary differential equations representing the energy exchanges among the different scales of motion. Each kind of motion is assumed to be describable with a limited number of shape parameters. The shape assumptions for the mean flow, waves, and turbulence required to perform the radial integrals in the energy equations are discussed next.

Mean flow. - We describe the mean flow in terms of the momentum thickness Θ. The mean flow profile is the two-stage hyperbolic tangent profile proposed by Michalke (ref. 22).

For $\Theta < 0.08$,

$$U(r,\Theta) = \begin{cases} 1 & \text{for} \quad 0 \le r \le 1 - \frac{\delta}{2} \\ \frac{1}{2}\left\{1 + \tanh\left[\frac{1}{2\Theta}(1 - r)\right]\right\} & \text{for} \quad 1 - \frac{\delta}{2} < r < \infty \end{cases} \qquad (22)$$

For $\Theta > 0.08$,

$$U(r,\Theta) = \frac{1}{2}\left\{1 + \tanh\left[\frac{1}{4\Theta}\left(\frac{1}{r} - r\right)\right]\right\} \quad \text{for} \quad 0 \le r \le \infty$$

This profile fits the experimental data (e.g., refs. 23 and 24) for the mean flow development between the jet exit and the fully developed region.

The mean flow is thus characterized by the momentum thickness θ rather than by the axial distance x. Therefore functional dependency on x in the integrals involved in the energy equations will be replaced by θ.

Random turbulence. - The radial distribution of the turbulent stresses is assumed to be given by a Gaussian profile in the form

$$\left.\begin{aligned} \overline{u_i' u_j'} &= a_{ij}\, E(x)\, G(\theta) \exp(-\eta^2) \\ \text{where} \qquad \eta^2 &= \frac{(r-1)^2}{\theta^2 C} \end{aligned}\right\} \tag{23}$$

This assumption is consistent with Lau's (ref. 25) findings based on correlating a large set of axial velocity fluctuations of unexcited jets over an extended range of jet operating conditions. The term $E(x)$ is the turbulence energy, and a_{ij} and C are constants given by

$$a_{11} = 1 \qquad a_{22} = a_{33} = 0.5 \qquad a_{12} = 0.33 \qquad a_{13} = a_{23} = 0 \quad \text{and} \quad C = 20 \tag{24}$$

This model is similar to that used by Mankbadi and Liu (ref. 6) and by Mankbadi (ref. 7), but it has been modified to account for a given turbulence level in the potential core. Within the potential core, the turbulence level is determined by its initial value at the exit of the jet. A normalization function $G(\theta)$ renders the fine-grained turbulence energy $E(x)$ over a section of the jet. Thus,

$$\left.\begin{aligned} E(x) &= \int_0^\infty \bar{q}(r\, dr) \\ \text{and} \qquad G(\theta) &= 1 \left(\int_0^\infty \exp(-\eta^2) r\, dr + T_o \right) \end{aligned}\right\} \tag{25}$$

for $\theta < 0.08$ and $T_o = 0$.

For $\theta > 0.08$ and $T_o = 0.5\, \overline{u_{oc}'^2}(1 - \theta/0.08)^2$, $\overline{u_{oc}'^2}$ is the initial turbulence intensity at the center of the jet exit.

This turbulence model is based on quasi-steady assumptions in which data from steady-flow experiments are used to model the turbulence at unsteady conditions. However, $E(x)$ is determined later on from the nonlinear interactions. The experimental data thus provide only the radial shape and the ratios between the stresses. The shape and ratios may vary under excitation at high frequencies. However, the interest here is within the jet column mode, the so-called preferred frequencies, which in general are lower than those of the shear layer instability frequencies. Therefore, for this range of frequencies

it is logical to assume that the ratios of the turbulent stresses are given by their corresponding values for the steady-state case.

The viscous dissipation in the turbulence energy equation is related to the small-scale turbulence as

$$\bar{\varepsilon} = \frac{a_2 \bar{q}^{3/2}}{\delta} \tag{26}$$

where $a_2 = 1.5$.

In the present system of variables δ is replaced by Θ where $\delta = a_3\Theta$ and $a_3 = 4.4$.

Wave components. - The momentum equation for each wave component mn is obtained by subtracting the time-averaged momentum equation from the mn-phase averaged momentum equation:

$$\frac{\partial \tilde{u}_{i,mn}}{\partial t} + \bar{U}_j \frac{\partial \tilde{u}_{i,mn}}{\partial x_j} + \tilde{u}_{j,mn} \frac{\partial \bar{U}_i}{\partial x_j} - \frac{\delta_{i2}}{r}\left(\tilde{r}_{\phi\phi,mn} + \langle \tilde{w}^2 \rangle_{mn} - \overline{\tilde{w}^2} + 2\bar{w}\,\tilde{w}_{mn}\right)$$

$$+ \frac{\delta_{i3}}{r}\left(\langle \tilde{w}\tilde{v} \rangle_{mn} - \overline{\tilde{w}\tilde{v}} + \tilde{r}_{\phi r,mn} + \bar{V}\tilde{w}_{mn} + \bar{W}\tilde{v}_{mn}\right)$$

$$= -\frac{\partial \tilde{P}_{mn}}{\partial x_i} - \frac{\partial}{\partial x_j^*}\left(\langle \tilde{u}_i \tilde{u}_j \rangle_{mn} - \overline{\tilde{u}_i \tilde{u}_j} + \tilde{r}_{ij,mn}\right)$$

$$+ \frac{1}{Re}\left[\nabla^2 \tilde{u}_{i,mn} - \frac{\delta_{i2}}{r^2}\left(\tilde{v}_{mn} - 2\frac{\partial \tilde{w}_{mn}}{\partial \phi}\right) - \frac{\delta_{i3}}{r^2}\left(\tilde{w}_{mn} - 2\frac{\partial \tilde{v}_{mn}}{\partial \phi}\right)\right] \tag{27}$$

where δ_{ij} is Kroneker's delta.

If this equation is linearized and the terms containing $\tilde{r}_{ij}$ are neglected, it can be simplified to the linear stability equation:

$$\frac{\partial \tilde{u}_i}{\partial t} + \bar{U}_j \frac{\partial \tilde{u}_i}{\partial x_j} + \tilde{u}_j \frac{\partial \bar{U}_i}{\partial x_j} = -\frac{\partial \tilde{p}}{\partial x_i} + \frac{1}{Re}\left[\nabla^2 \tilde{u}_i - \frac{\delta_{i2}}{r^2}\left(\tilde{v} + 2\frac{\partial \tilde{w}}{\partial \phi}\right) - \frac{\delta_{i3}}{r^2}\left(\tilde{w} - 2\frac{\partial \tilde{v}}{\partial \phi}\right)\right] \tag{28}$$

The shape assumptions for the wave components follow those of previous works (refs. 6, 7, 26, and 27) in assuming that the Fourier coefficient u_{mn} in equation (2) can be separated into an amplitude that is a function of x and a shape that is a function of r at a given location along the jet. In these previous works, the complex radial shape was obtained from the linear stability equation. In Mankbadi (ref. 7) the amplitude was obtained from the nonlinear analysis while its phase angle was obtained from the linear analysis.

Experimental (refs. 17 and 28) and theoretical (refs. 15, 16, and 29) investigations have indicated that nonlinear wave interactions are highly dependent on the phase angles between the waves. Furthermore, the experimental

data of Mankbadi, Raman, and Rice (ref. 28) clearly indicate that the development of these phase angles is a highly nonlinear process. Therefore, previous shape assumptions for the wave components are modified to

$$\tilde{u}_{i,mn} = \left|A_{mn}(x)\right|\hat{u}_{i,mn}(r,\theta)\exp\left[i\psi_{mn}(x) - i\omega_m t + iN_n\phi\right] + cc \qquad (29)$$

The radial shapes $\hat{u}(r,0)$ are given as the eigenfunctions of the locally parallel linear stability equation as before. However, now both the amplitudes A_{mn} and the phase angles ψ_{mn} are determined from the nonlinear analysis.

As pointed out before, the linearized form of the momentum equation for the mn-wave is simply the linear stability equation. Therefore, to a first approximation $\psi(x)$ is given by $\exp(i_0 \int^x \alpha(\xi)\, d\zeta)$ where α is the complex wave number corresponding to the frequency ω. The radial shapes $\hat{u}(r,\theta)$ and the corresponding complex wave numbers are obtained from the local linear stability theory. The fact that the radial shapes of the waves can be obtained from the locally parallel stability theory was confirmed experimentally by Strange and Crighton (ref. 30) and Wygnanski and Petersen (ref. 11).

The solution of the inviscid stability equation follows that given by Michalke (ref. 22). In the damped region, a complex contour is used for the numerical integration as in Mankbadi and Liu (ref. 6). The eigenfunctions are normalized in such a way as to render A_{mn} the energy of the mn-wave in a section of the jet. The arguments of the complex eigenfunctions are normalized by taking the phase angle of $\hat{u}$ to be zero at the jet centerline. The phase angle is therefore that of the streamwise wave velocity at the jet centerline.

Wave-induced stresses. - When the full form of the $\tilde{r}_{ij}$ equations is linearized, it reduces to the same form as that of a single mn-wave component. Therefore, it is modeled following Mankbadi and Liu (ref. 6) for the interaction between the single-frequency component and the random turbulence. Based on the linearized form, it can be shown that $\tilde{r}_{ij}$ takes the form

$$\tilde{r}_{ij,mn} = \left|A_{mn}(x)\right|E(x)\hat{r}_{ij,mn}\exp\left[i(\psi(x) - \omega_m t + iN_n\phi\right] + cc \qquad (30)$$

The closure model for the wave-induced stresses follows that of the mean turbulence quantities. Details of the model are given in Mankbadi and Liu (ref. 6). The modeled linearized equation for $\hat{r}_{ij}$ is

$$
\begin{aligned}
i\alpha(U-c)&\begin{bmatrix}\hat{r}_{xx}\\ \hat{r}_{rr}\\ \hat{r}_{\phi\phi}\\ \hat{r}_{xr}\\ \hat{r}_{x\phi}\\ \hat{r}_{r\phi}\end{bmatrix}
\quad
\underbrace{\begin{bmatrix}2\hat{r}_{xr}\\ 0\\ 0\\ \hat{r}_{rr}\\ \hat{r}_{r\phi}\\ 0\end{bmatrix}U'}_{\text{production}}
+\frac{1}{T}
\underbrace{\begin{bmatrix}\hat{r}_{xx}-\frac{1}{3}\hat{r}_{kk}\\ \hat{r}_{rr}-\frac{1}{3}\hat{r}_{kk}\\ \hat{r}_{\phi\phi}-\frac{1}{3}\hat{r}_{kk}\\ \hat{r}_{xr}\\ \hat{r}_{x\phi}\\ \hat{r}_{r\phi}\end{bmatrix}}_{\text{pressure-velocity correlation}}
+\frac{1}{2}a_{12}U'
\underbrace{\begin{bmatrix}\hat{r}_{kk}\\ \hat{r}_{kk}\\ \hat{r}_{kk}\\ 0\\ 0\\ 0\end{bmatrix}}_{\text{dissipation}}
\\
&\underbrace{\qquad\qquad}_{\text{advection by the mean flow}}
\end{aligned}
\qquad\qquad (31)
$$

$$
\begin{aligned}
=-\hat{v}&\begin{bmatrix}R'_{xx}\\ R'_{rr}\\ R'_{\phi\phi}+2R_{\phi\phi}/r\\ R'_{xr}\\ 0\\ 0\end{bmatrix}
-\frac{\hat{w}}{r}
\underbrace{\begin{bmatrix}0\\ 0\\ 0\\ 0\\ R_{xr}\\ -2R_{\phi\phi}+R_{rr}\end{bmatrix}}_{\text{advection of mean stresses by wave}}
-\underbrace{\begin{bmatrix}2(R_{xx}i\alpha+R_{xr}D)\hat{u}\\ 2(R_{xr}i\alpha+R_{rr}D)\hat{v}\\ 2R_{\phi\phi}in\hat{w}/r\\ (R_{xx}i\alpha+R_{xr}D)\hat{v}+(R_{xr}i\alpha+R_{rr}D)\hat{u}\\ (R_{xx}i\alpha+R_{xr}D)\hat{w}+R_{\phi\phi}in\hat{u}/r\\ (R_{xr}i\alpha+R_{rr}D)\hat{w}+R_{\phi\phi}in\hat{v}/r\end{bmatrix}}_{\text{work done by the mean stresses against wave rates of strain}}
\end{aligned}
$$

where $T^{-1}=-1.445\partial U/\partial r>0$ is the time scale for return to isotropy, $\hat{r}_{kk}=\hat{r}_{xx}+\hat{r}_{rr}+\hat{r}_{\phi\phi}$, and $'$ and D indicate differentiation with respect to r.

Nonlinear Interaction Equations

With the shape assumptions introduced in equation (3), the energy equations (eqs. (7) to (9)) can be integrated across the jet to yield the following system of simultaneous ordinary differential equations.

The mean flow momentum thickness $\theta(x)$ is given by

$$
\frac{1}{2}\frac{dI_{MA}}{d\theta}\frac{d\theta}{dx}=-I_{MT}E_t-\sum_{m,n}I_{MW,mn}E_{mn} \qquad (32)
$$

The turbulence kinetic energy $E_t(x)$ is given by

$$\frac{d}{dx}\left(I_{TA}E_t\right) = I_{MT}E_t + \sum_{m,n} I_{TW,mn}E_{mn}E_t - I_{\varepsilon}E_t^{3/2} \tag{33}$$

The energy of the mn-wave $E_{mn}(x)$ is given by

$$\frac{d}{dx}\left(I_{WA,mn}E_{mn}\right) = I_{WM}E_{mn} - I_{WT,mn}E_{mn}E_t + WW_{mn} \tag{34}$$

and the phase angle $\psi_{mn}(x)$ is given by

$$E_{mn}I_{WA}\frac{d\psi_{mn}}{dx} = \pi S_{mn}E_{mn} + I'_{WM}E_{mn} + WW'_{mn} \tag{35}$$

In this system of equations, I represents an integral that is, in general, a function of the momentum thickness θ, frequency ω, and the azimuthal number N considered. In the mean flow equation (32), I_{MA} is the mean flow advection integral given by

$$I_{MA}(\theta) = \int_0^{\infty} \bar{U}^3 \, r \, dr \tag{36}$$

The first term on the right side of equation (32) is the mean flow production of the turbulence, and the second term is the production of each individual wave. The mean flow production integrals of the random turbulence and the wave component, I_{MT} and I_{MW}, respectively, are given by

$$I_{MT}(\theta) = -a_{12}G(\theta)\int_0^{\infty} \exp(-\eta^2)\,\frac{\partial \bar{U}}{\partial r}\, r \, dr \tag{37}$$

and

$$I_{MW,mn}(\theta,\omega_m,N_n) = -2\int_0^{\infty} Re\left(\hat{u}_{mn}\hat{v}^*_{mn}\right)\frac{\partial U}{\partial r}\, r \, dr \tag{38}$$

where Re indicates the real part.

In the turbulence energy equation (33), I_{TA} is the integral of the turbulence advection by the mean flow given by

$$I_{MT}(\theta) = G(\theta)\left[\int_0^{\infty} U \exp(-\eta^2) r \, dr + T_o\right] \tag{39}$$

The first term on the right side of equation (33) is the turbulence produced by the mean flow. The second term is the turbulence energy exchanged with the waves, and the last term is the viscous dissipation.

The integrals I_{WT} and I_ε are given by

$$I_{WT}(\Theta,\omega_m,N_n) = -2\int_0^\infty Re\Big\{\hat{r}_{xx,mn}(i\alpha\hat{u}_{mn}) + \hat{r}^*_{rr,mn}\hat{v}'_{mn} + \hat{r}_{\phi\phi,mn}\left(\frac{in\hat{w}_{mn}}{r} + \frac{\hat{v}_{mn}}{r}\right) + \hat{r}^*_{r\phi,mn}\left[\frac{in\hat{v}_{mn}}{r} + r\left(\frac{\hat{w}_{mn}}{r}\right)'\right] + \hat{r}^*_{x\phi}\left(\frac{in\hat{u}^*_{mn}}{r} + i\alpha\hat{w}_{mn}\right) + r^*_{xr}(i\alpha\hat{v}_{mn} + \hat{u}')\Big\}r\,dr \qquad (40)$$

and

$$I_\varepsilon(\Theta) = (a_2/a_3\,\Theta)G^{3/2}(\Theta)\left[\int_0^\infty \exp\left(-\tfrac{3}{2}\,\eta^2\right)r\,dr + T_\varepsilon\right] \qquad (41)$$

where $'$ denotes differentiation with respect to r,

$$T_\varepsilon = \left(\overline{u'^2_{oc}}\right)^{3/2}(1 - 12.5\,\Theta)$$

In the energy equation for the mn-wave (eq. (34)), I_{WA} is the integral for the wave advection by the mean flow:

$$I_{WA}(\Theta,\omega_m,N_n) = \int_0^\infty U\left(\left|\hat{u}_{mn}\right|^2 + \left|\hat{v}_{mn}\right|^2 + \left|\hat{w}_{mn}\right|^2\right)r\,dr$$

The first term on the right side of equation (34) is the wave production by the mean flow. The second term is the interaction with the turbulence. The last term in equation (34) is the interaction of the mn-wave with other waves. The term WW_{mn} is actually the sum of the interactions of the mn-wave with other existing waves. It is given here only for waves with frequencies of ω, 2ω, and 4ω and with azimuthal numbers of 0 and 1. Thus, for these six waves WW_{mn} takes the form

$$
\left.
\begin{aligned}
WW_{10} &= -E_{10}\sqrt{E_{20}}\, w_{10,10,20} + \sqrt{E_{21}E_{11}E_{10}}\, w_{21,11,10} \\
WW_{20} &= E_{10}\sqrt{E_{20}}\, w_{10,10,20} - E_{20}\sqrt{E_{30}}\, w_{20,20,30} + \sqrt{E_{31}E_{21}E_{20}} \\
WW_{30} &= E_{20}\sqrt{E_{30}}\, w_{20,20,30} \\
WW_{11} &= -\sqrt{E_{10}E_{11}E_{21}}\, w_{10,11,21} - \sqrt{E_{21}E_{11}E_{10}}\, w_{21,11,10} \\
WW_{21} &= \sqrt{E_{10}E_{11}E_{21}}\, w_{10,11,21} - \sqrt{E_{20}E_{21}E_{31}}\, w_{20,11,21} - \sqrt{E_{31}E_{21}E_{20}}\, w_{31,21,20} \\
WW_{31} &= \sqrt{E_{20}E_{21}E_{31}}\, w_{20,21,31}
\end{aligned}
\right\} \quad (42)
$$

where

$$
w_{ij,k\ell,mn} = 2\left|I_{ij,k\ell,mn}\right|\cos\left(\psi_{ij} + \psi_{k\ell} - \psi_{mn} + \sigma_{ij,k\ell,mn}\right) .
$$

and where $\sigma_{ij,k\ell,mn}$ is the argument of $I_{ij,k\ell,mn}$ and

$$
\left.
\begin{aligned}
I_{10,10,20} &= \int_0^\infty \hat{u}^*_{i,10}\hat{u}^*_{j,10}\,\frac{\partial \hat{u}_{i,20}}{\partial x_j}\,r\,dr \\
I_{20,20,30} &= \int_0^\infty \hat{u}^*_{i,20}\hat{u}^*_{j,20}\,\frac{\partial \hat{u}_{i,30}}{\partial x_j}\,r\,dr \\
I_{10,11,21} &= \int_0^\infty \left(\hat{u}^*_{i,10}\hat{u}^*_{j,11}\,\frac{\partial \hat{u}_{i,21}}{\partial x_j} - \frac{\hat{v}_{10}\hat{w}_{11}\hat{w}_{21}}{r}\right) r\,dr \\
I_{20,21,31} &= \int_0^\infty \left(\hat{u}^*_{i,20}\hat{u}^*_{j,21}\,\frac{\partial \hat{u}_{i,31}}{\partial x_j} - \frac{\hat{v}_{21}\hat{w}_{21}\hat{w}_{31}}{r}\right) r\,dr \\
I_{21,11,10} &= \int_0^\infty \hat{u}^*_{i,21}\hat{u}^*_{j,11}\,\frac{\partial \hat{u}_{i,10}}{\partial x_j}\,r\,dr \\
I_{21,21,20} &= \int_0^\infty \hat{u}^*_{i,31}\hat{u}^*_{j,21}\,\frac{\partial \hat{u}_{i,20}}{\partial x_j}\,r\,dr
\end{aligned}
\right\} \qquad (43)
$$

The phase-development equation (35) is obtained in a manner similar to that of Mankbadi (ref. 16). The Strouhal number S is defined as $\omega_{mn}d/(2\pi U_e)$, where d is the nozzle diameter; I'_{WM} is given by

$$
I'_{WM,mn} = -\mathcal{I}m\int_0^\infty \hat{u}^*_{mn}\hat{v}_m\,\frac{\partial \bar{U}}{\partial r}\,r\,dr \qquad (44)
$$

and WW'_{mn} is identical to WW_{mn} (eqs. (42) and (43)) except that it is the imaginary part, and therefore the $\cos(\ )$ term is replaced by $\sin(\ )$: that is,

$$
w'_{ij,k\ell,mn} = 2\left|I_{ij,k\ell,mn}\right|\sin\left(\psi_{ij} + \psi_{k\ell} - \psi_m + \sigma_{ij,k\ell,mn}\right) \qquad (45)
$$

This system of equations (eqs. (32) to (35)) is subject to the initial conditions at $x = 0$: $\Theta(0)$, $E_t(0)$, and $E_{mn}(0)$, and to the initial phase angle $\psi_{mn}(0)$ with respect to a given reference.

TWO-FREQUENCY EXCITATIONS

Before we present the results for multiple frequency excitations, we first compare the predictions of the present formulation with corresponding

experimental data for the case of a turbulent round jet excited at two frequencies. Under two-frequency excitations, control can be exercised over the initial energy levels as well as over the initial phase difference between the two excitation components.

The solution of the system of nonlinear equations depends on the specified initial levels. Therefore, to compare the present predictions to the experimental results, we obtain the initial conditions from the corresponding experiment.

The calculated fundamental and subharmonic components at Strouhal numbers of 0.3 and 0.6 are shown in figure 2 for several initial phase angles. When only two waves are present, there is one initial phase-difference angle β between them. The initial momentum thickness is 0.026, and $E_o = 0.0001$. The initial energies of the fundamental (S = 0.6) and the subharmonic (S = 0.3) are taken such that the initial instability axial velocity components at the jet centerline are 1.2 and 0.6 percent of the jet exit velocity. These values were based on Bradley's data (ref. 13). Figure 2 shows that the fundamental is not as sensitive to the phase difference as the subharmonic is. Bradley measured the spectral amplitudes that were proportional to the energies (ref. 13). His measured data behave similar to the predictions of figure 2. The fundamental is less dependent than the subharmonic on the initial phase angle. Bradley's measured maximum subharmonic amplification occurs at $\beta = 180°$, and the minimum subharmonic amplification occurs at $\beta = 0°$ (ref. 13), which is the same as the predicted results of figure 2.

Figure 3 compares the calculated centerline phase-averaged velocities with the corresponding data of Arbey and Ffowcs-Williams (ref. 18). The Strouhal numbers are 0.3 and 0.6, and $E_o = 0.00001$. The initial centerline velocity of the S = 0.3 component is 1.5 percent of the jet exit velocity; the initial centerline velocity of the S = 0.6 component is 0.38 that of the S = 0.3, as in the experiment. At S = 0.3, the calculated peaks occur further downstream than the data peaks (fig. 3(a)). However, the calculated peaks are at the same velocity level as the data peaks. Both the theory and the experiment indicate that the S = 0.3 component peak increases when β changes from 0° to 180°. The calculated phase-averaged velocities at S = 0.6 (fig. 3(b)) also have the same features, the same level of amplification, and the same dependency on the phase angle as the measured data. The measured component increases again after it decays, which is probably due to its interaction with other frequency components - a mechanism which is not allowed here since frequency components other than S = 0.3 and S = 0.6 are forced to be zero.

The dependency of the subharmonic amplification on the initial phase angle is shown in figure 4 for Strouhal numbers of 0.2 and 0.4. The calculations are shown in figure 4(a), and the corresponding measurements of Raman and Rice (ref. 12) are shown in figure 4(b). In both cases the velocities are normalized by the maximum attainable peak of the subharmonic. The initial levels are $u_{fo} = 7$ percent, $u_{so} = 0.5$ percent, and $E_o = 0.005$. At this high level of excitation the acoustic decay is dominant in the first half diameter (ref. 12). Therefore, Tam and Morris's (ref. 31) correction for the acoustic interaction is used in the first half diameter. Figure 4 shows that both the measurements and the theory predict a strong influence of the phase angle. The subharmonic peak can be reduced to about one-third of its maximum attainable value depending on the initial phase difference between the two waves.

The calculated and measured momentum thicknesses are shown in figure 5 for the two-frequency excited and the unexcited cases. The initial conditions are the same as those of figure 4. Figure 5 shows that two-frequency excitation can considerably increase the jet mixing. However, the enhanced momentum thickness is only weakly dependent on the phase angle. This indicates that the direct role of the subharmonic in controlling the mixing of turbulent jets is less pronounced than its role in advancing the mixing of laminar jets (refs. 5 and 16). However, the subharmonic can still have a strong indirect role in the mixing process since it can control the background turbulence that, in turn, controls the mixing process.

If both the fundamental and subharmonic initial energy levels are large, their respective energy drain from the mean flow is also large. Therefore, the wave-wave interactions become less significant. The dependency of the wave amplification on the initial phase angles should be less pronounced. This phenomenon is demonstrated in figure 6 where both waves have the same high initial energy levels, $\tilde{u}_{fo} = \tilde{u}_{so} = 3$ percent. The Strouhal numbers are 0.3 and 0.6. The present predictions of the subharmonic peak as a function of the initial phase difference are shown in figure 6(a), and the corresponding data of Raman and Rice (ref. 12) are shown in figure 6(b). The theory and observations both indicate the same weak dependency on the phase angle.

According to the present analysis, the wave-wave interactions are dependent on the energy levels. Therefore, increasing the initial energy level of the fundamental, while keeping that of the subharmonic small, should increase the peak of the subharmonic. The calculated subharmonic peak as a function of the initial level of the fundamental is shown in figure 7(a). The Strouhal numbers are 0.2 and 0.4, the initial velocity of the subharmonic is $1/15^{th}$ that of the fundamental, and the initial phase angle is kept at 270°. The corresponding data of Raman and Rice (ref. 12) are shown in figure 7(b). Both theory and experiment indicate that the peak of the subharmonic increases as the fundamental's energy level increases. The subharmonic reaches a saturation value of about 20 percent.

MULTIFREQUENCY EXCITATION

The data of Moore (ref. 32) and Raman, Rice, and Mankbadi (ref. 33) indicate that within the Strouhal number range 0.2 to 1.0, a forced-wave component amplifies along the jet and can influence the growth rate of the jet. Therefore, in the present study three frequencies, corresponding to Strouhal numbers of 0.2, 0.4, and 0.8, are considered. These Strouhal numbers were chosen to cover jet excitability in the experimentally indicated range referred to as the "jet column mode" (ref. 9). The next two sections present the results for multifrequency excitation in the axisymmetric mode. In the first section results for interactions with equal initial levels of all waves are presented. In the succeeding section, results for variable ratios of initial energy levels are presented.

Multifrequency Forcing at Equal Energy Levels

In this section, the initial energy levels of all waves are equal, and the initial momentum thickness is taken to be 0.012. Since the focus here is on

highly turbulent jets, the initial turbulence energy level is taken to be relatively high $E_t(0) = 0.005$. With three interacting waves there are two initial phase differences. The phase difference between $S = 0.2$ and $S = 0.4$ is β_{12} and that between $S = 0.4$ and $S = 0.8$ is β_{23}.

Figure 8 shows the energy peak of each wave component normalized by its initial value as a function of the phase differences. The initial energy level (which is equal for the three waves) is varied from 10^{-6} to 5×10^{-3} in figure 8(a) to (d). This range of initial energy levels corresponds to initial wave velocities of roughly 0.001 to 0.07 U_e. A comparison of part (a) of figure 8 with parts (b) to (d) indicates that the dependency on the phase angle increases as the initial energy level increases. This trend is expected since the wave-wave interaction is a nonlinear process. At low levels (fig. 8(a)), each wave grows almost independently of the other waves. At higher energy levels (fig. 8(c)), the energy peak can be doubled depending on the phase angle, indicating strong nonlinear interactions.

A comparison of parts (a) to (d) of figure 8 also indicates that the maximum attainable normalized peak decreases as the initial energy levels increase. This fact is demonstrated in figure 9, which shows the maximum attainable peak (depending on the combination of phase differences) as a function of the initial energy level. Figure 9 indicates that at low initial energy levels the peak varies in accordance with the linear theory. However, the rate of growth decreases with higher energy levels, and saturation conditions are reached around energy levels of 0.005 to 0.01. Further increases in the initial energy level damp the forced component.

The maximum attainable (depending on the phase angles) momentum thickness along the jet is shown in figure 10 for several initial energy levels. This figure shows that the higher the initial energy level, the greater the mixing rate enhancement due to excitation. Since we are interested in enhancing the mixing and since the saturation is limited as shown in figure 9, $E_o = 0.005$ seems to be the optimum value. Therefore, multifrequency forcing at $E_o = 0.005$ is examined further in figures 11 to 21.

To examine the role of multifrequency forcing on jet mixing, we use three phase-difference combinations but keep the other initial conditions fixed (figs. 11 to 16). In figures 11 and 12 the phase differences β_{12} and β_{23} are 0° and 90°, respectively. Figure 11 shows the energies of the three frequency components and indicates that $S = 0.4$ is the most amplified component along the jet. The mean flow productions of the wave components and of the turbulence are shown in figure 12. The sum of these productions determines the growth rate, and hence the mixing rate, of the jet. The mean flow production of the turbulence for the unexcited case is also shown in figure 12. Figure 12 shows that the production of the three waves is important in the initial region of the jet. But further downstream beyond $x = d$, the production of the turbulence dominates.

In figures 13 and 14 the phase angles β_{12} and β_{23} are 90° and 180°, respectively. The energies of the waves are shown in figure 13, which indicates that the $S = 0.4$ component is less amplified than it is in figure 11. The mean flow productions are shown in figure 14, which also indicates that the turbulence production is the dominant mechanism beyond $x = d$. The case of $\beta_{12} = 270°$ and $\beta_{23} = 180°$ is shown in figures 15 and 16. Figure 15 shows that for this combination of phase differences $S = 0.2$ is the most amplified

component along the jet. The corresponding mean flow productions are shown in figure 16. This figure also shows that turbulence production is the dominant mechanism. A comparison of the turbulence produced by the mean flow for the excited and unexcited cases (fig. 16) shows that multifrequency excitation can considerably increase the random turbulence produced by the mean flow.

The momentum thickness along the jet is shown in figure 17 for the three pairs of phase-difference combinations that were presented in figures 11 to 16. Figure 17 shows considerable enhancement in the momentum thickness for the three cases considered. In the case of $\beta_{12} = 90°$ and $\beta_{23} = 0°$, the momentum thickness around $x = 4d$ is greater than for $\beta_{12} = 90°$ and $\beta_{23} = 180°$ because the $S = 0.4$ component is amplified more in the former case than in the latter case (fig. 11 versus fig. 13). Figure 17 also shows that the momentum thickness is most enhanced when $\beta_{12} = 270°$ and $\beta_{23} = 180°$. For this case $S = 0.2$ is the most amplified component (fig. 15). This low Strouhal number wave has the longest streamwise lifespan, and therefore it is the most effective in enhancing mixing at downstream locations.

Figure 18 shows the turbulence energy along the jet for the phase-difference combinations in figure 17. The turbulence energy for the unexcited case is also shown on figure 18. The turbulence is enhanced because of the forcing. Note also that forcing at different phase-difference combinations has the same effect on the turbulence as it does on the momentum thickness (fig. 17).

In laminar jets, where turbulence is negligible, the growth rate is dictated by only the production of the waves. Therefore subharmonic amplification or damping would have a pronounced effect on the jet growth rate (refs. 5 and 16). For turbulence jets where the growth rate is governed by the production of the turbulence and the waves, the situation is different. As indicated by figures 12, 14, and 16, the turbulence production is the dominant mechanism in controlling the growth rate. The direct role of wave amplification in the growth rate is not pronounced for the turbulent jets as it is for the laminar jets. The forced waves, however, enhance the random turbulence and therefore still play an indirect role in the mixing process.

The turbulence enhancement of the random turbulence that was shown in figure 18 is evident in the early experiments of Binder and Favre-Marinet (ref. 3). The mechanism of turbulence enhancement under multifrequency excitation is examined here. The energy pumped into the turbulence by the waves and the mean flow are shown in figures 19 to 21 for three different pairs of phase-difference combinations. These figures show that turbulence enhancement under excitation is a result of a direct and an indirect mechanism. In the direct mechanism, the imposed waves decay by dissipating their energy into the background turbulence (the second term in the turbulence energy equation, eq. (33)). In the second indirect mechanism, the wave acts as a catalyst that enhances the mean flow production of the turbulence. Note that in figures 19 to 21, the mean flow production of the turbulence for the excited case is much higher than that in the unexcited case. The mean flow production of the turbulence is proportional to the local level of the turbulence energy (the first term in the turbulence energy equation (eq. (33))). Therefore, wave-produced enhancement in E_t further increases the mean flow production of the turbulence $E_t I_{MT}$. Thus, the mean flow production of the turbulence is increased

by excitation. In figure 21, the S = 0.2 component, which has a long streamwise lifespan, is amplified. This wave keeps pumping energy to the turbulence for a long distance along the jet and causes the greatest enhancement in the mean flow production of the turbulence.

Forcing at Variable Initial Energy Ratios

In the previous section we considered the case of forcing at equal energy levels. In the next section, we consider the case when one of the waves has an initial energy level that is one order of magnitude lower than the other two. In the succeeding section, we consider the case when one of the waves has an initial energy level that is one order of magnitude higher than the other two.

One wave initially weaker than the other waves. - The peak of the three waves as a function of the initial phase angles are shown in figure 22. In figure 22(a) the S = 0.8 wave is initially an order of magnitude smaller than the other two. In figure 22(b), the S = 0.4 wave is the weak one, while in figure 22(c), the S = 0.2 wave is the weak one. In figure 22(a), the S = 0.8 component is negligible with respect to the other two waves. Therefore the S = 0.2 and S = 0.4 waves behave as in the case of two-frequency excitation. When S = 0.4 is the weak wave, figure 22(b), it still amplifies considerably. The S = 0.4 wave has a Strouhal number near that of the most amplified wave. Furthermore, this wave interacts directly with the other two waves. Considerable wave interactions occur that can amplify the S = 0.4 wave to the same level as that of the other two waves. When S = 0.2 is the weak wave, the S = 0.2 wave is not amplified and the other two waves, S = 0.4 and S = 0.8, behave as if the third wave were not present at all (fig. 22(c)).

The turbulence energy along the jet is shown in figure 23 for the initial energy ratios of figure 22. Note that the figure indicates that the S = 0.2 component must be present to have a considerable effect on the turbulence because of the long streamwise lifespan of the S = 0.2 component, as indicated before. The figure also shows a greater effect on the turbulence when the two high-level waves are S = 0.8 and 0.4, instead of S = 0.2 and 0.4. As indicated before, when the S = 0.8 and S = 0.2 waves are high, they excite the S = 0.4 component and thus act effectively as three-frequency excitation. This mechanism is not present when the two high-amplitude waves are S = 0.2 and 0.4.

The momentum thickness along the jet is shown in figure 24 for the same initial values as in figure 23. Figure 24 shows that the effect of excitation on the momentum thickness follows the same pattern as the effect of excitation on the turbulence. This indicates again that it is the turbulence that controls the mixing enhancement.

One wave initially higher than the other waves. - One wave was given a high initial energy level of $E_o = 0.005$ while the other waves were kept an order of magnitude lower (i.e., $E_o = 0.0005$). Although this is a case of multifrequency interactions, it can represent the experimental situation when only one frequency is forced. In an unexcited jet, there are several stability components that are naturally present. In an excited jet, the excitation wave can interact with other naturally present waves at other frequencies and amplify

them (e.g., ref. 9). The low initial energy level of $E_o = 0.0005$ can represent that of the naturally present waves.

Figure 25 shows the energy peak for each frequency component as a function of the phase-difference angles. In figure 25(a) the S = 0.8 component is the high-amplitude wave. It produces some amplification of the S = 0.4 component, which in turn can enhance the S = 0.2 component. In figure 25(b), the S = 0.4 component is the high-amplitude wave. It can enhance the S = 0.2 component if the phase difference between them is 270°, but it has a negligible effect on the S = 0.8 component. In figure 25(c), the S = 0.2 component is the high-amplitude wave. The S = 0.4 component interacts with both the S = 0.2 component and the slightly amplified S = 0.8 component.

The turbulence energy is shown in figure 26. The initial phase angles that produced the greatest effect on the turbulence were chosen for a given high-amplitude excitation at a given frequency. At $x < d$, the S = 0.8 component produces the highest effect on the turbulence. The S = 0.8 component amplifies very close to the jet exit and therefore is effective in pumping energy from the mean flow to the turbulence in this region. If one considers the region $x > d$, the S = 0.2 component is the most effective in pumping energy from the mean flow to the turbulence. The S = 0.2 component peaks further downstream and has the longest streamwise lifespan. Therefore, the high-frequency components are effective in enhancing the turbulence in the initial region of the jet while the low-frequency components are effective further downstream. The momentum thickness for the cases in figure 26 are shown in figure 27. Figure 27 shows that the effect of frequency on the momentum thickness follows the effect of the frequency on the turbulence. This again indicates that the turbulence is the effective mechanism for turbulence enhancement of excited turbulent jets.

Figures 28 to 33 show the energy of the frequency components and the corresponding turbulence productions for the three cases presented in figures 26 and 27. In figure 28, S = 0.8 is initially the highest component; it amplifies in the initial region of the jet. Figure 29 shows that the S = 0.8 wave component pumps considerable energy into the turbulence in the initial region of the jet. As a result of this energy transfer, the mean flow production of the turbulence is also enhanced. When the high energy is in the S = 0.4 component (figs. 30 and 31), the behavior is similar to that when S = 0.8 is the high component. However, the high S = 0.4 component peaks further downstream. As a result, the enhancement of the mean flow production of the turbulence in figure 31 is delayed in comparison with the corresponding enhancement in figure 29. Note also that when S = 0.4 is the high-amplitude component, it dampens the S = 0.8 component (fig. 30). Therefore the S = 0.8 component plays a negligible role in pumping energy from the mean flow to the turbulence. When S = 0.2 is the high-amplitude component, the other frequencies are amplified slightly (fig. 32). In figure 33 all waves pump energy to the turbulence. Furthermore, because of its long streamwise lifespan, the S = 0.2 component keeps pumping energy to the turbulence along the jet. As a result of this continuous increase in the turbulence energy, the mean flow production of the turbulence is also considerably enhanced. Apparently, if the S = 0.2 component can be amplified through its interaction with other frequency components, it can have a considerable effect on the turbulence.

CONCLUSIONS

The interactions among several stability waves in a turbulent round jet were examined based on the integrated energy in a section of the jet for the different scales of motion. The present formulations indicate that if only axisymmetric wave components are present, two frequency components with high amplitudes can interact with each other as well as with other background-frequency components and can generate an enormous number of other frequency components in the axisymmetric mode. If the frequency components present are only in the first-helical mode, two frequency components in the first-helical mode cannot interact directly with each other or with other first-helical frequency components. However, if both the axisymmetric and the first-helical component are simultaneously present with frequency components related by fundamental-subharmonic relations, mixed interactions between the axisymmetric and the helical mode occur. These mixed interactions amplify other frequencies in both the axisymmetric and the helical modes.

The present predictions for two-frequency axisymmetric excitation produce results consistent with those from several published experiments. When a jet is excited at fundamental and subharmonic frequencies with the fundamental level higher than that of the subharmonic, the amplification of the subharmonic greatly depends on the initial phase difference between the two waves. This dependency on the initial phase angle becomes less pronounced if both components have high initial energy levels. Two-frequency excitation enhances the momentum thickness in accordance with observations.

If a jet is forced with multifrequency components of equal initial energy levels, the nonlinear process depends on the initial level. At low energy levels, nonlinear interactions are negligible, and each wave behaves as if the others were not present. Increasing the initial energy level equally for all waves results in considerable nonlinear interactions. At much higher initial levels, a saturation condition is reached in which the waves can no longer amplify each other. Increasing the initial energy level increases the momentum thickness of the jet until the saturation condition is reached.

Examining the energy exchanges at high forcing levels of equal magnitudes for all the waves indicates several interesting features. The enhancement in the momentum thickness is dominated by the mean flow turbulence production, rather than by the fundamental-subharmonic interactions as in the laminar case. Multifrequency forcing of the jet enhances the turbulence through two mechanisms. In the direct mechanism, the imposed waves decay by dissipating their energy into the background turbulence. In the second indirect mechanism, the wave acts as a catalyst that enhances the mean flow production of the turbulence. The turbulence produced by the mean flow is proportional to the local level of the turbulence energy. Therefore, wave-produced enhancement in the turbulence energy further increases the turbulence produced by the mean flow. Thus, excitation enhances the mean flow production of the turbulence.

The role of the frequency on the nonlinear process was examined by varying the ratios of initial energy levels between the frequency components. Two-frequency excitation at high and low frequencies can result in considerable amplification of the intermediate frequencies. Thus, proper two-frequency excitation can be as effective as three-frequency excitation.

By taking the initial energy level of one of the frequency components to be much larger than the others, we demonstrated that high frequencies are effective in pumping energy from the mean flow to the turbulence. Low frequencies have longer streamwise lifespans and therefore are more effective in pumping energy from the mean flow to the turbulence at locations further downstream.

APPENDIX - SYMBOLS

A	amplitude
a_{ij}, C	constants
cc	complex conjugate
D	differentiated with respect to r
d	nozzle diameter
dis	turbulence dissipation
E(x)	energy
E_o	initial energy level
E_p	energy peak
E_t	turbulence energy
G(Θ)	normalization function
I	integral that is a function of Θ, ω, and N
I_{MA}	mean flow advection integral
I_{MT}	mean flow production integral of the random turbulence
I_{MW}	mean flow production integral of the wave component
I_{TA}	turbulence advection integral
I_{WA}	wave advection integral
Im	imaginary
g,i,j,k,ℓ,m,n	variables
MT	mean flow production of turbulence
MW	mean flow production of wave components
N	azimuthal number

P	pressure
Q	kinetic energy of the wave
q	kinetic energy of the turbulence
R	nozzle radius
Re	Reynolds number
$\mathcal{Re}$	real part
r	radical coordinate
$\tilde{r}_{ij,mn}$	wave-induced stresses
S	Strouhal number
T^{-1}	time scale for return to isotropy
T_o	$0.5\ u'^2_{oc}(1 - \Theta/0.08)^2$
t	time
U	velocity
$\bar{U}_i(\underline{x})$	time-averaged motion
U_p	peak velocity
u	streamwise velocity
$u'_i(\underline{x},r)$	background, fine-scale random turbulence
$\tilde{u}$	periodic component
$\tilde{u}_f$	periodic component at fundamental frequency
$\tilde{u}_i(\underline{x},t)$	periodic, organized, large-scale wave-shaped motion
V	mean radial velocity
v	radial velocity
W	azimuthal velocity
WT	energy transfer between the waves and the turbulence
WW	interaction between one wave and other existing waves
w	azimuthal velocity (angular velocity)
x	axial distance

α	complex wave number corresponding to frequency ω
β	initial phase-difference angle
β_{12}	initial phase difference between S_1 and S_2
β_{23}	initial phase difference between S_2 and S_3
δ	displacement thickness
δ_{ij}	Kroneker's delta
ϵ	viscous dissipation
θ	momentum thickness
ρ	fluid density
σ	argument of I
ϕ	azimuthal angle
ψ	phase angle
ω	frequency

Subscripts:

e	jet exit
f	fundamental frequency
i,j,k,ℓ,m,n	variables
MA	mean flow advection
MT	mean turbulence
o	initial conditions
oc	exit, centerline
s	subharmonic
sp	subharmonic peak
TA	turbulence advection
t	turbulence (p. 28)
WA	wave advection
x	axial coordinate

Superscripts:

$\overline{\quad}$	usual time average of the flow quantity
~	wavelike
*	complex conjugate
^	eigenfunction
'	differentiated with respect to r

REFERENCES

1. Miksad, R.W.: Experiments on the Nonlinear Stages of Free Shear-Layer Transition. J. Fluid Mech., vol. 56, pt. 4, Dec. 1972, pp. 695-719.

2. Miksad, R.W.: Experiments on the Nonlinear Interactions in the Transition of a Free Shear Layer. J. Fluid Mech., vol. 59, pt. 1, June 1973, pp. 1-21.

3. Binder, G.; and Favre-Marinet, M.: Mixing Improvement in Pulsating Turbulent Jets. Fluid Mechanics of Mixing, E.M. Uram, and V.M. Goldsmidt, eds., ASME, 1973, pp. 167-172.

4. Binder, G.; and Favre-Marinet, M.: Some Characteristics of Pulsating or Flapping Jets. Unsteady Turbulent Shear Flows, M. Roger, J. Cousteix, and R. Houdeville, eds., Springer-Verlag, 1981, pp. 370-379.

5. Ho, C.M.; and Huang, L.S.: Subharmonics and Vortex Merging in Mixing Layer. J. Fluid Mech., vol. 119, June 1982, pp. 443-473.

6. Mankbadi, R.R.; and Liu, J.T.C.: A Study of the Interactions Between Large-Scale Coherent Structures and Fine-Grained Turbulence in a Round Jet. Philos. Trans. R. Soc. London A, vol. 298, no. 1443, Jan. 1981, pp. 541-602.

7. Mankbadi, R.R.: On the Interaction Between Fundamental and Subharmonic Instability Waves in a Turbulent Round Jet. J. Fluid Mech., vol. 160, Nov. 1985, pp. 385-419.

8. Winant, C.D.; and Browand, F.K.: Vortex Pairing: The Mechanism of Turbulent Mixing Layer Growth at Moderate Reynolds Number. J. Fluid Mech., vol. 63, pt. 2, Apr. 1974, pp. 237-255.

9. Zaman, K.B.M.Q.; and Hussain, A.K.M.F.: Vortex Pairing in a Circular Jet Under Controlled Excitation, Part 1. General Jet Response. J. Fluid Mech., vol. 101, pt. 3, Dec. 1980, pp. 449-491.

10. Ho, C.M.; and Huerre, P.: Perturbed Free Shear Layers. Annual Review of Fluid Mechanics, Vol. 16, M. Van Dyke, J.V. Wehausen, and J.L. Lumley, eds., Annual Review Inc., Palo Alto, CA, 1984, pp. 365-424.

11. Wygnanski, I.; and Petersen, R.A.: Coherent Motion in Excited Free Shear Flows. AIAA J., vol. 25, Feb. 1987, pp. 201-213.

12. Raman, G.; and Rice, E.J.: Subharmonic and Fundamental High-Amplitude Excitation of an Axisymmetric Jet. AIAA Paper 89-0993, Mar. 1989 (NASA TM-101946).

13. Bradley, T.A.: The Effects of Forcing on the Near Field Development of a Jet. M.S. Thesis, Univ. of Notre Dame, IN, 1987.

14. Patnaik, P.C.; Sherman, F.S.; and Corcos, G.M.: A Numerical Simulation of Kelvin-Hemholtz Waves of Finite Amplitude. J. Fluid Mech., vol. 73, pt. 2, Jan. 1976, pp. 215-240.

15. Riley, J.J.; and Metcalfe, R.W.: Direct Numerical Simulation of Perturbed Mixing Layer. AIAA Paper 80-0274, Jan. 1980.

16. Mankbadi, R.R.: The Effect of Phase-Difference on the Spreading Rate of a Jet. AIAA J., vol. 24, Dec. 1986, pp. 1941-1948.

17. Zhang, Y.Q.; Ho, C.M.; and Monkewitz, P.: The Mixing Layer Forced by Fundamental and Subharmonic. Laminar-Turbulent Transition. V.V. Kozlov, ed., Springer-Verlag, 1985, pp. 385-395.

18. Arbey, H.; and Ffowcs-Williams, J.E.: Active Cancellation of Pure Tones in an Excited Jet. J. Fluid Mech., vol. 149, Dec. 1984, pp. 445-454.

19. Hussain, A.K.M.F.; and Reynolds, W.C.: The Mechanics of an Organized Wave in Turbulent Shear Flow. J. Fluid Mech., vol. 41, pt. 2, Apr. 1970, pp. 241-258.

20. Kendall, J.M.: The Turbulent Boundary Layer Over a Wall With Progressive Surface Waves. J. Fluid Mech., vol. 41, pt. 2, Apr. 1970, pp. 259-281.

21. Cohen, J.; and Wygnanski, I.: The Evolution of Instabilities in the Axisymmetric Jet. Part 2. The Flow Resulting From the Interaction Between Two Waves. J. Fluid Mech., vol. 176, Mar. 1987, pp. 221-235.

22. Michalke, A.: Instabiluitat Eines Kompressiblen Runden Freistrahls Ubter Berucksichtingung des Einflusses der Strahlgrenzschichttdicke. Z. Flugwiss. vol. 19, no. 819, 1971, pp. 319-328. (Translation, NASA TM-75190.)

23. Freymouth, P.: On Transition in a Separated Laminar Boundary Layer. J. Fluid Mech., vol. 25, pt. 4, Aug. 1966, pp. 683-704.

24. Strange, P.J.R.: Spinning Modes in Orderly Jet Structured Jet Nozzle. Ph.D. Thesis, University of Leeds, England, 1981.

25. Lau, J.C.: Mach Number and Temperature Effects on Jets. AIAA Paper 78-1152, July 1978.

26. Ko, D.R.S.; Kubota, T.; and Lees, L.: Finite Disturbance Effect on the Stability of a Laminar Incompressible Wave Behind a Flat Plate. J. Fluid Mech., vol. 40, pt. 2, Feb. 1970, pp. 315-341.

27. Liu, J.T.C.; and Lees, L.: Finite-Amplitude Instability of the Compressible Laminar Wake. Strongly Amplified Disturbances. Phys. Fluids, vol. 13, no. 12, Dec. 1970, pp. 2932-2938.

28. Mankbadi, R.R.; Raman, G.; and Rice, E.J.: On the Conditions for Resonance Interactions of Instability Waves in the Axisymmetric Jet. NASA TM-101477, 1989.

29. Monkewitz, P.A.: Subharmonic Resonance, Pairing and Shredding in the Mixing Layer. J. Fluid Mech., vol. 188, Mar. 1988, pp. 223-252.

30. Strange, P.J.R.; and Crighton, D.G.: Spinning Modes on Axisymmetric Jets. J. Fluid Mech., vol. 134, Sept. 1983, pp. 231-245.

31. Tam, C.K.W.; and Morris, P.J.: Tone Excited Jets, Part V: A Theoretical Model and Comparison with Experiment. J. Sound Vibration, vol. 102, pt. 1, Sept. 8, 1985, pp. 119-151.

32. Moore, C.J.: The Role of Shear-Layer Instability Waves in Jet Exhaust Noise. J. Fluid Mech., vol. 80. pt. 2, Aug. 1977, pp. 321-367.

33. Raman, G.; Rice, E.J.; and Mankbadi, R.R.: Saturation and the Limit of Jet Mixing Enhancement by Single Frequency Plane Wave Excitation: Experiment and Theory. AIAA Paper 88-3613, July 1988 (NASA TM-100882).

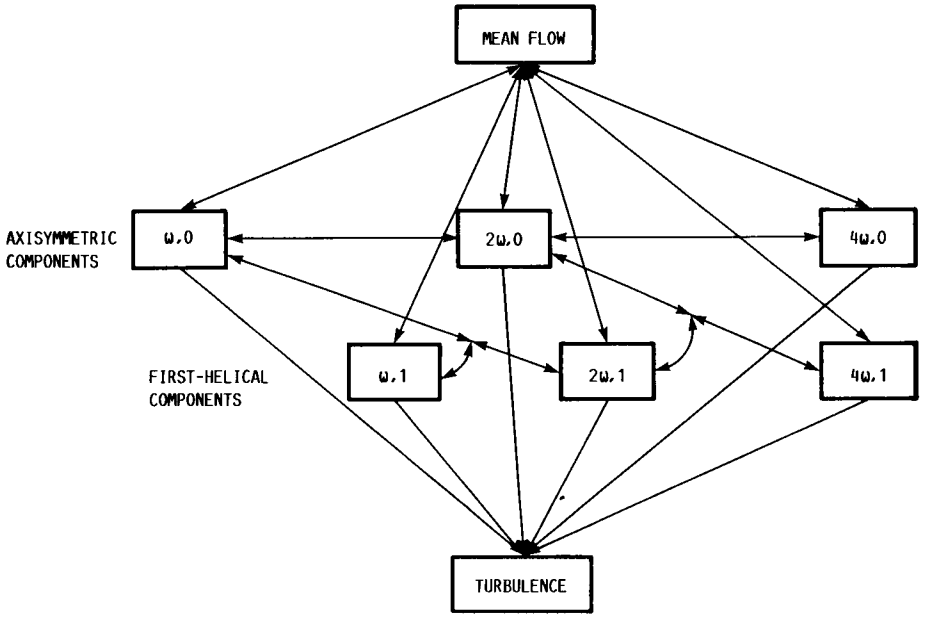

FIGURE 1. - ENERGY EXCHANGES.

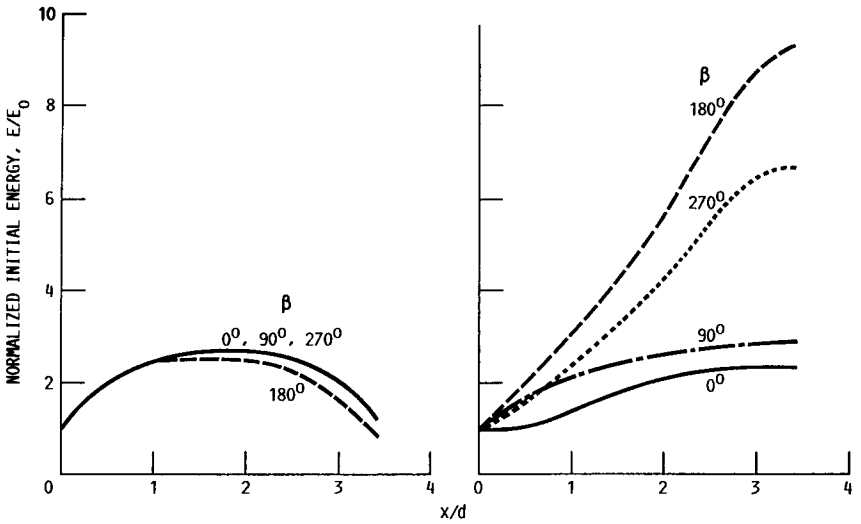

(a) STROUHAL NUMBER, S, 0.6. (b) STROUHAL NUMBER, S, 0.3.

FIGURE 2. - DEPENDENCY OF STABILITY ON THE INITIAL PHASE ANGLES, β.

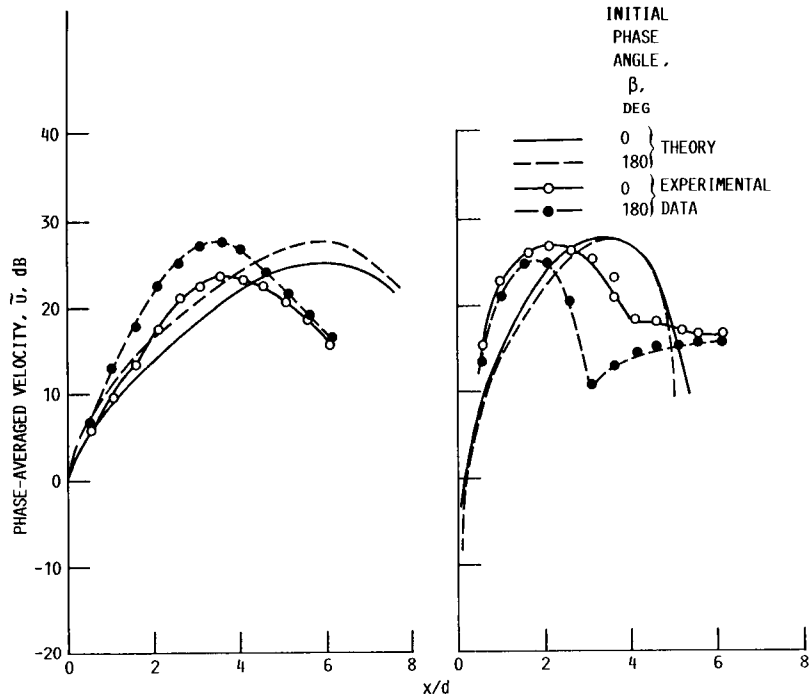

(a) STROUHAL NUMBER, S, 0.3. (b) STROUHAL NUMBER, S, 0.6.

FIGURE 3. - COMPARISON BETWEEN CALCULATED PHASE-AVERAGED CENTERLINE VELOCITIES AND ARBEY AND FFOWCS-WILLIAMS' DATA (REF. 16).

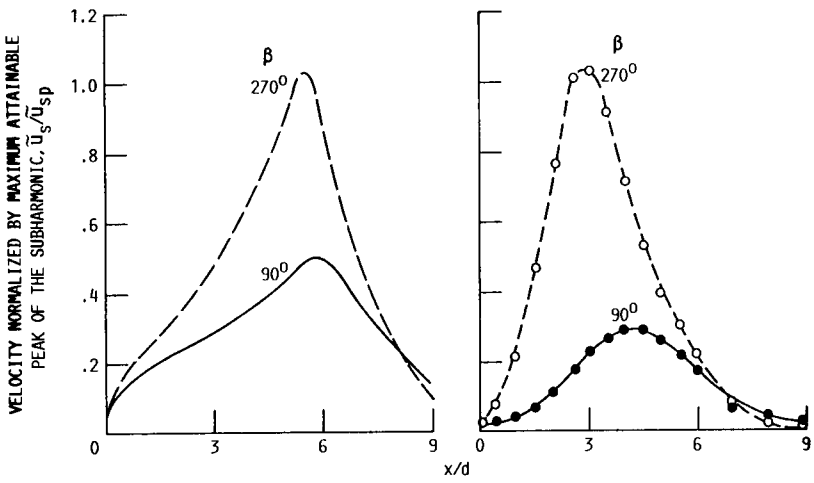

(a) CALCULATIONS. (b) EXPERIMENTAL DATA OF RAMAN AND RICE (REF. 10).

FIGURE 4. - DEPENDENCE OF SUBHARMONIC AMPLIFICATION ON THE INITIAL PHASE ANGLE, β, AT STROUHAL NUMBER PAIR 0.4 AND 0.2.

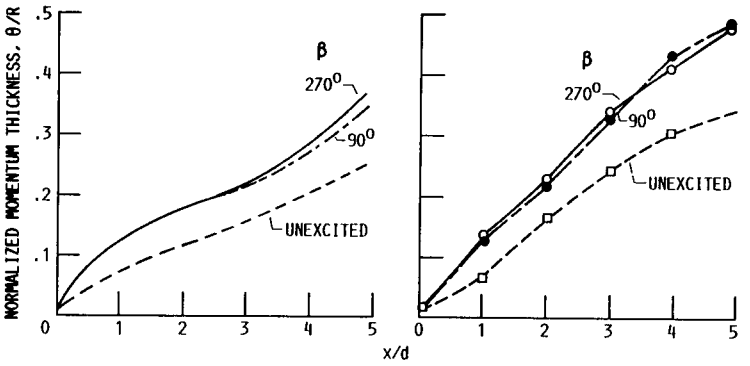

(a) CALCULATIONS.

(b) EXPERIMENTAL DATA OF MANKBADI, RAMAN, AND RICE (REF. 26).

FIGURE 5. - DEVELOPMENT OF MOMENTUM THICKNESS UNDER TWO-FREQUENCY EXCITATION AND FOR THE UNEXCITED CASE.

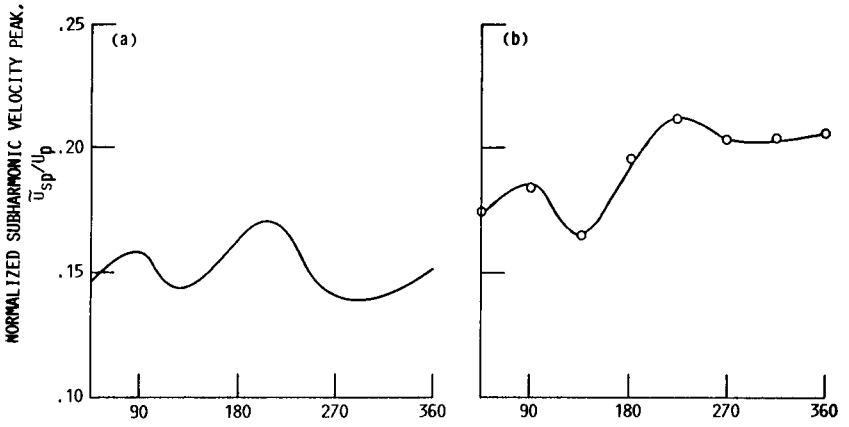

(a) THEORY.

(b) EXPERIMENTAL DATA OF RAMAN AND RICE (REF. 10).

FIGURE 6. - DEPENDENCY OF SUBHARMONIC PEAK ON THE PHASE ANGLE AT HIGH LEVELS OF BOTH FUNDAMENTAL AND SUBHARMONIC.

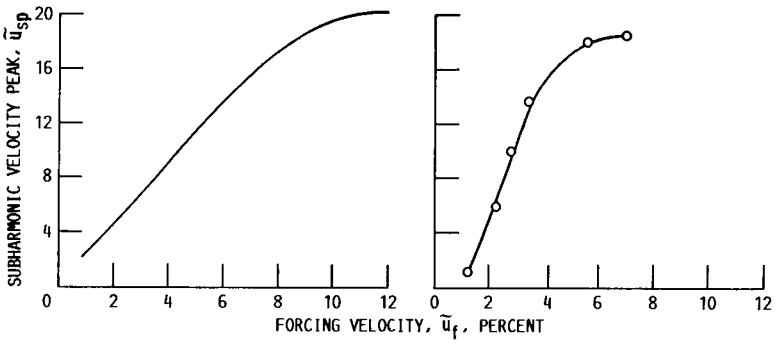

(a) THEORY.

(b) EXPERIMENTAL DATA OF RAMAN AND RICE (REF. 10).

FIGURE 7. - DEPENDENCY OF SUBHARMONIC PEAK ON THE FORCING LEVEL AT STROUHAL NUMBERS OF 0.2 AND 0.4.

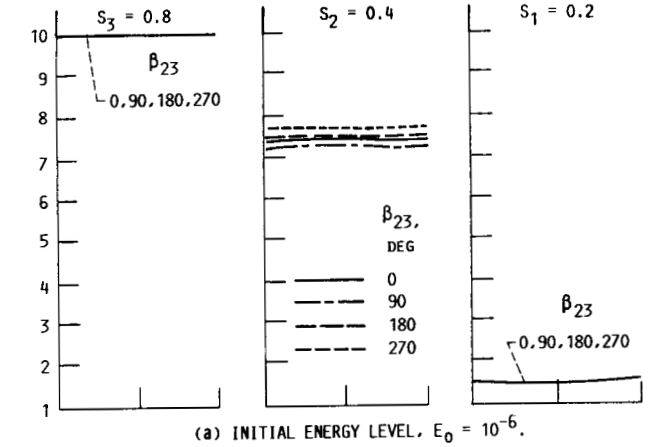

(a) INITIAL ENERGY LEVEL, $E_0 = 10^{-6}$.

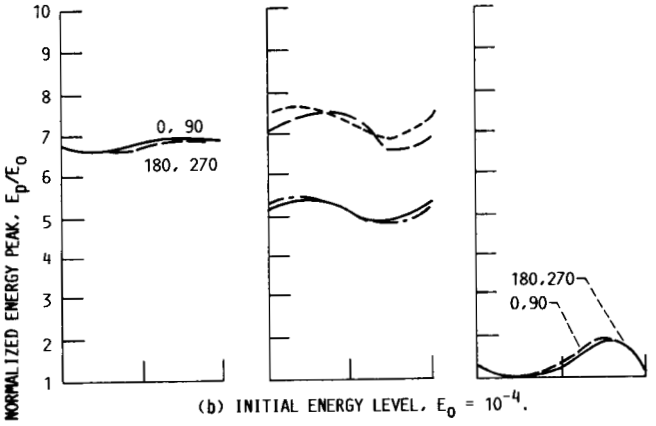

(b) INITIAL ENERGY LEVEL, $E_0 = 10^{-4}$.

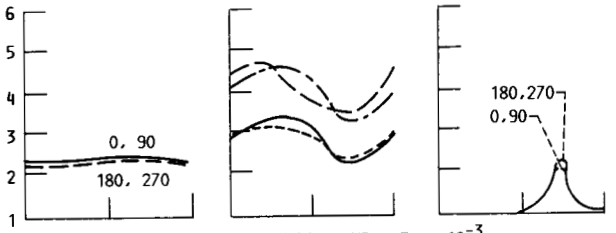

(c) INITIAL ENERGY LEVEL, $E_0 = 10^{-3}$.

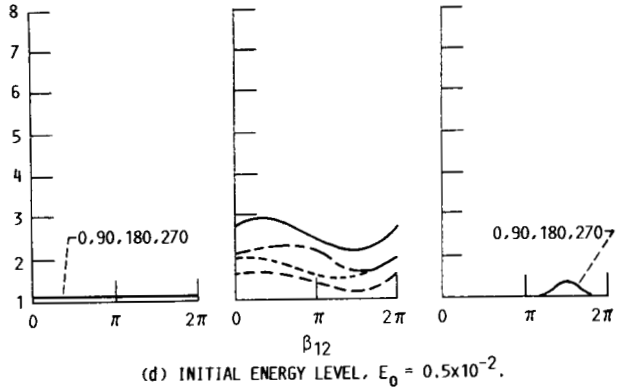

(d) INITIAL ENERGY LEVEL, $E_0 = 0.5 \times 10^{-2}$.

FIGURE 8. - EFFECT OF PHASE DIFFERENCES, β_{12} AND β_{23}, ON PEAK OF EACH FREQUENCY COMPONENT (THREE STROUHAL NUMBERS, S). EQUAL INITIAL ENERGY LEVELS.

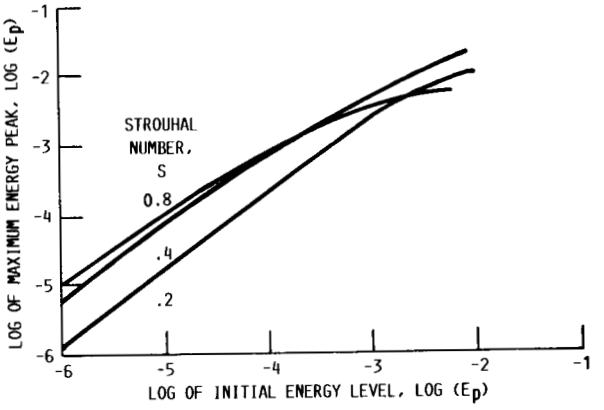

FIGURE 9. - MAXIMUM ATTAINABLE PEAK AS FUNCTION OF THE INITIAL ENERGY LEVEL.

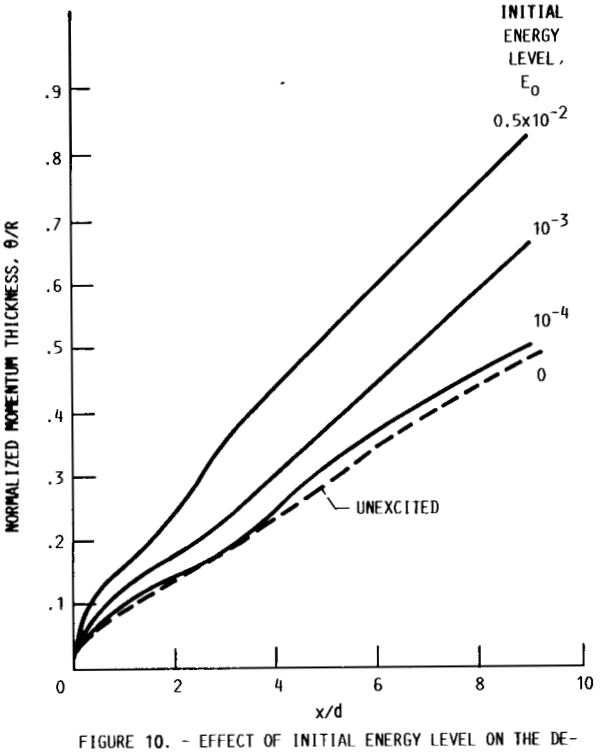

FIGURE 10. - EFFECT OF INITIAL ENERGY LEVEL ON THE DEVELOPMENT OF THE MOMENTUM THICKNESS.

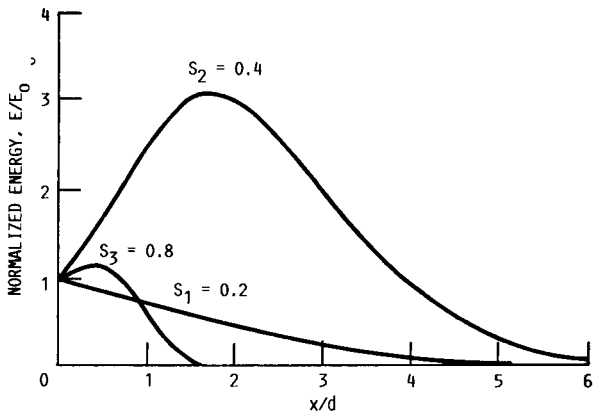

FIGURE 11. - DEVELOPMENT OF THE ENERGY OF EACH FREQUENCY COMPONENT (THREE STROUHAL NUMBERS, S) ALONG THE JET AT EQUAL INITIAL ENERGY LEVELS, $E_0 = 0.005$. INITIAL PHASE DIFFERENCES: $\beta_{12} = 90^0$; $\beta_{23} = 0^0$.

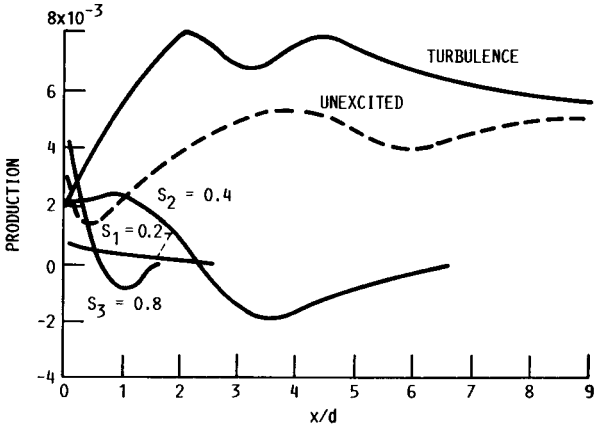

FIGURE 12. - MEAN FLOW ENERGY DRAIN TO THE WAVES (THREE STROUHAL NUMBERS, S) AND TURBULENCE AT EQUAL INITIAL ENERGY LEVELS, $E_0 = 0.005$. INITIAL PHASE DIFFERENCES: $\beta_{12} = 90^0$; $\beta_{23} = 0^0$.

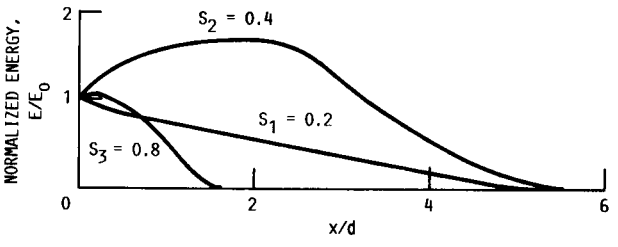

FIGURE 13. - DEVELOPMENT OF THE ENERGY OF EACH FREQUENCY COMPONENT (THREE STROUHAL NUMBERS, S) ALONG THE JET AT EQUAL INITIAL ENERGY LEVELS, $E_0 = 0.005$. INITIAL PHASE DIFFERENCES: $\beta_{12} = 90^0$; $\beta_{23} = 180^0$.

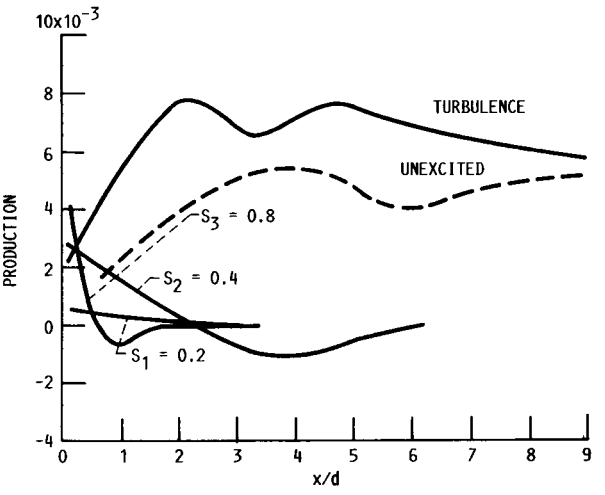

FIGURE 14. - MEAN FLOW ENERGY DRAIN TO THE WAVES (THREE STROUHAL NUMBERS, S) AND TURBULENCE AT EQUAL INITIAL ENERGY LEVELS, $E_0 = 0.005$. INITIAL PHASE DIFFERENCES: $\beta_{12} = 90^0$; $\beta_{23} = 180^0$.

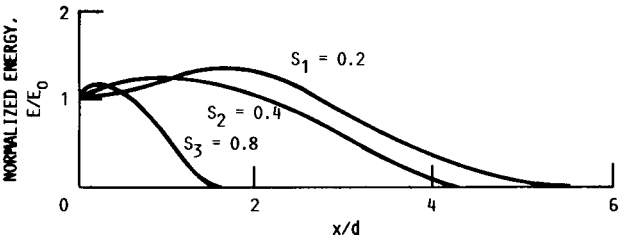

FIGURE 15. - DEVELOPMENT OF THE ENERGY OF EACH FREQUENCY COMPONENT (THREE STROUHAL NUMBERS, S) ALONG THE JET AT EQUAL INITIAL LEVELS, $E_0 = 0.005$. INITIAL PHASE DIFFERENCES: $\beta_{12} = 270^0$; $\beta_{23} = 180^0$.

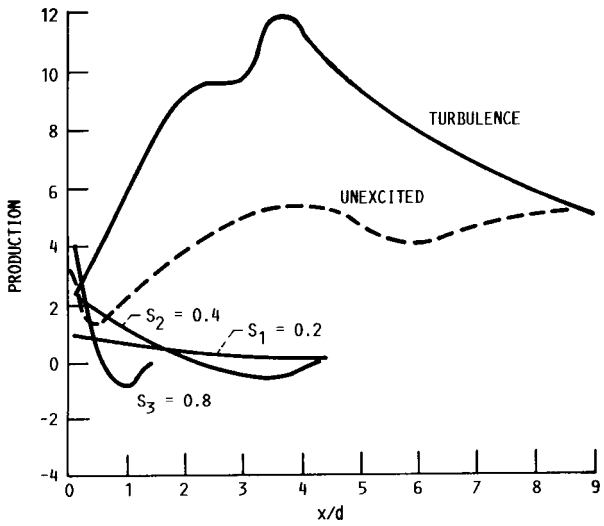

FIGURE 16. - MEAN FLOW ENERGY DRAIN TO THE WAVES (THREE STROUHAL NUMBERS, S) AND TURBULENCE AT EQUAL INITIAL ENERGY LEVELS, E_0 = 0.005. INITIAL PHASE DIFFERENCE, $\beta_{12} = 270^0$.

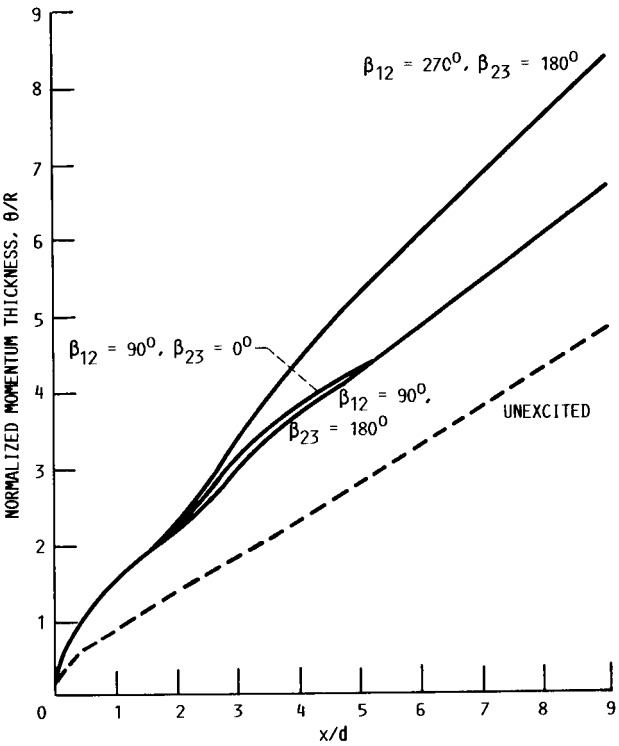

FIGURE 17. - EFFECT OF INITIAL PHASE DIFFERENCES (β_{12} AND β_{23}) ON THE MOMENTUM THICKNESS. EQUAL INITIAL ENERGY LEVELS, E_0 = 0.005.

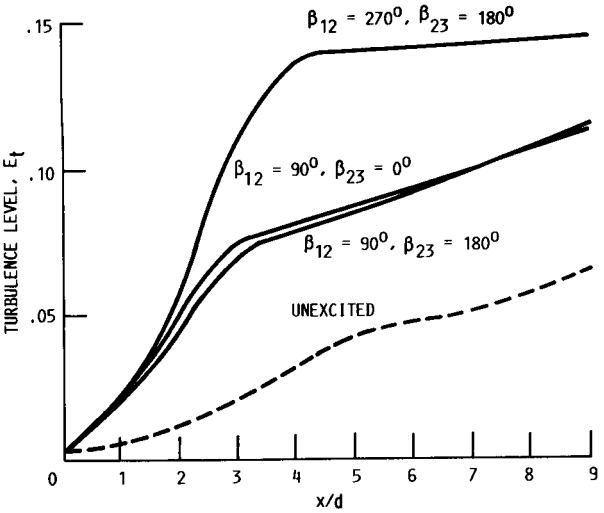

FIGURE 18. - EFFECT OF INITIAL PHASE DIFFERENCES, β_{12} AND β_{23}, ON THE TURBULENCE ENERGY. EQUAL INITIAL ENERGY LEVELS, E_0 = 0.005.

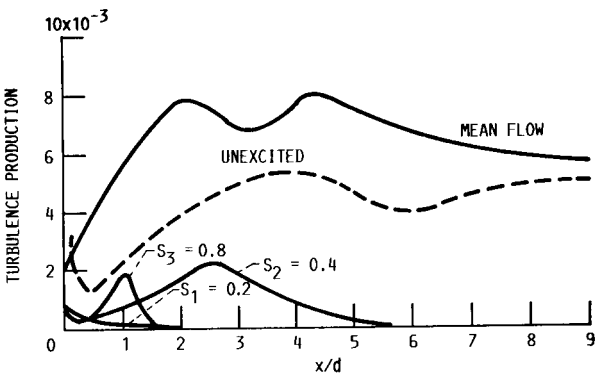

FIGURE 19. - TURBULENCE PRODUCTION BY THE MEAN FLOW AND WAVES. EQUAL INITIAL ENERGY LEVELS, E_0 = 0.005. INITIAL PHASE DIFFERENCES: $\beta_{12} = 90^0$; $\beta_{23} = 0^0$.

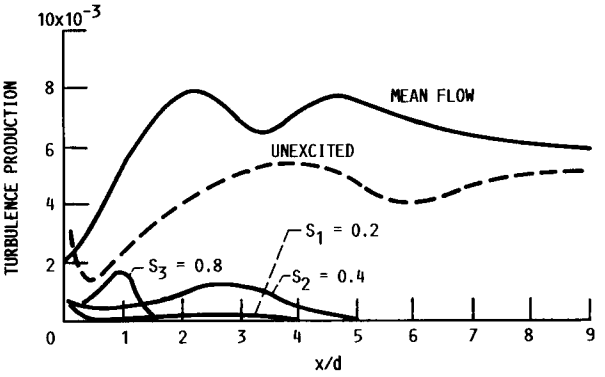

FIGURE 20. - TURBULENCE PRODUCTION BY THE MEAN FLOW AND WAVES (THREE STROUHAL NUMBERS, S). EQUAL INITIAL ENERGY LEVELS, E_0 = 0.005. INITIAL PHASE DIFFERENCES: $\beta_{12} = 90^0$; $\beta_{23} = 180^0$.

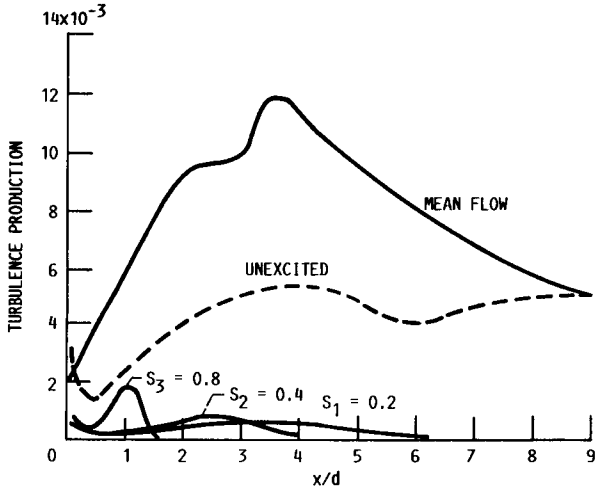

FIGURE 21. - TURBULENCE PRODUCTION BY THE MEAN FLOW AND WAVES (THREE STROUHAL NUMBERS, S). EQUAL INITIAL ENERGY LEVELS, E_0 = 0.005. INITIAL PHASE DIFFERENCES: $\beta_{12} = 270^0$; $\beta_{23} = 180^0$.

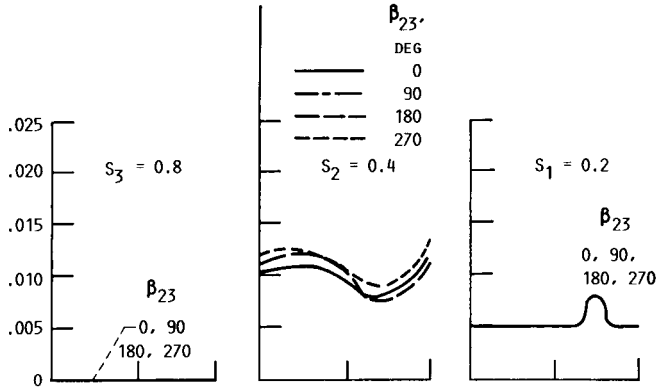

(a) INITIAL ENERGY LEVELS: $E_{10} = 0.005$; $E_{20} = 0.005$; $E_{30} = 0.0005$.

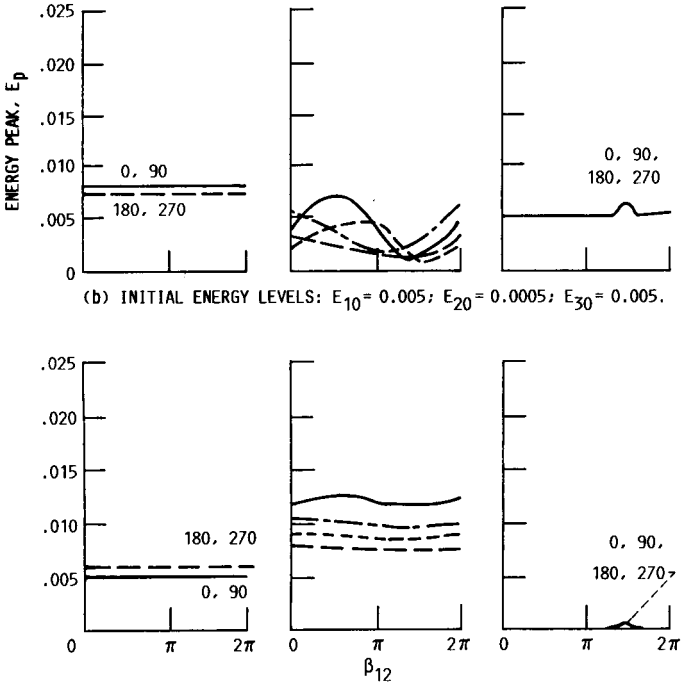

(b) INITIAL ENERGY LEVELS: $E_{10} = 0.005$; $E_{20} = 0.0005$; $E_{30} = 0.005$.

(c) INITIAL ENERGY LEVELS: $E_{10} = 0.0005$; $E_{20} = 0.005$; $E_{30} = 0.005$.

FIGURE 22. - EFFECT OF INITIAL PHASE DIFFERENCES, β_{12} AND β_{23}, ON THE PEAK OF EACH FREQUENCY COMPONENT (THREE STROUHAL NUMBERS, S). NONEQUAL INITIAL ENERGY LEVELS.

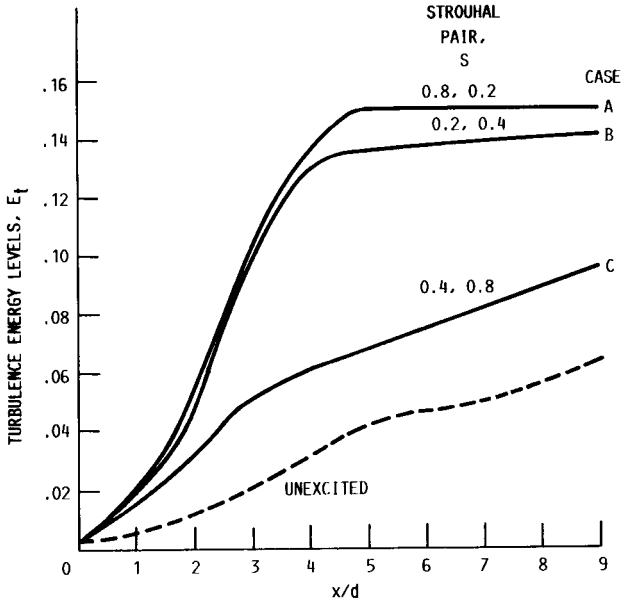

FIGURE 23. - TURBULENCE ENHANCEMENT UNDER VARIABLE RATIOS OF INITIAL ENERGY LEVELS. CASE A: INITIAL PHASE DIFFERENCES, $\beta_{12} = 270^0$; $\beta_{23} = 0^0$; INITIAL ENERGY LEVELS, $E_{10} = 0.005$; $E_{20} = 0.005$; $E_{30} = 0.0005$. CASE B: $\beta_{12} = 270^0$; $\beta_{23} = 0^0$; $E_{10} = 0.005$; $E_{20} = 0.0005$; $E_{30} = 0.005$. CASE C: $\beta_{12} = 270^0$; $\beta_{23} = 270^0$; $E_{10} = 0.0005$; $E_{20} = 0.005$; $E_{30} = 0.005$.

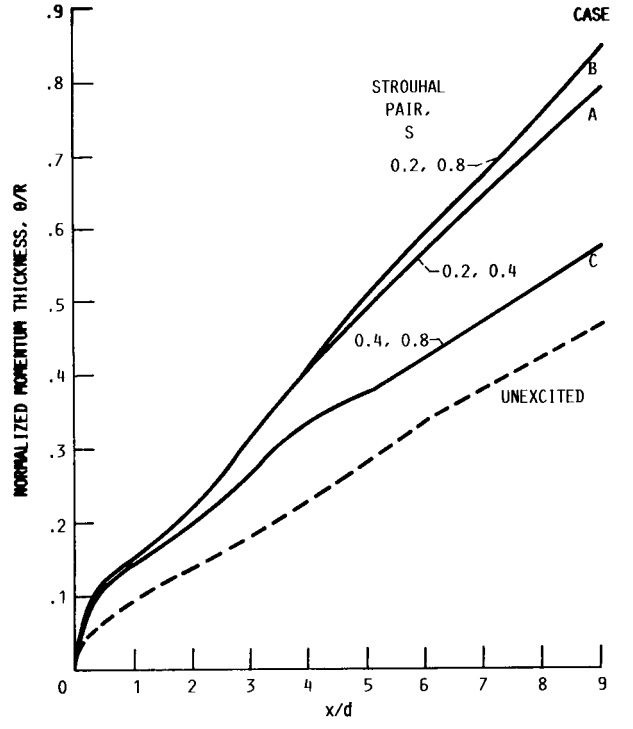

FIGURE 24. - MOMENTUM THICKNESS ENHANCEMENT UNDER VARIABLE RATIOS OF INITIAL ENERGY LEVELS. CASE A: INITIAL PHASE DIFFERENCES, $\beta_{12} = 270^0$; $\beta_{23} = 0^0$; INITIAL ENERGY LEVELS, $E_{10} = 0.005$; $E_{20} = 0.005$; $E_{30} = 0.0005$. CASE B: $\beta_{12} = 270^0$; $\beta_{23} = 0^0$; $E_{10} = 0.005$; $E_{20} = 0.0005$; $E_{30} = 0.005$. CASE C: $\beta_{12} = 270^0$; $\beta_{23} = 270^0$; $E_{10} = 0.0005$; $E_{20} = 0.005$; $E_{30} = 0.005$.

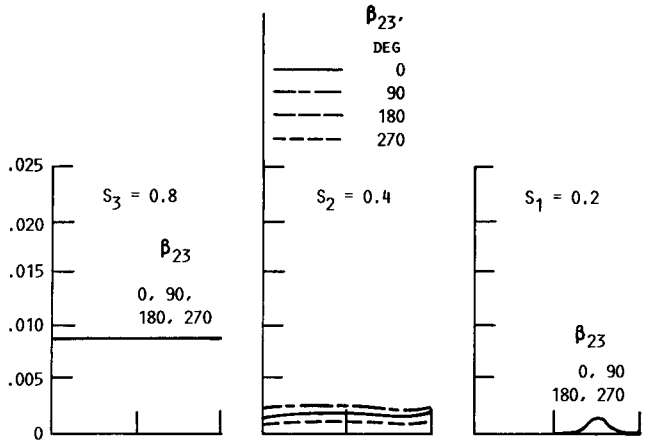

(a) INITIAL ENERGY LEVELS: $E_{10} = 0.0005$; $E_{20} = 0.0005$; $E_{30} = 0.005$.

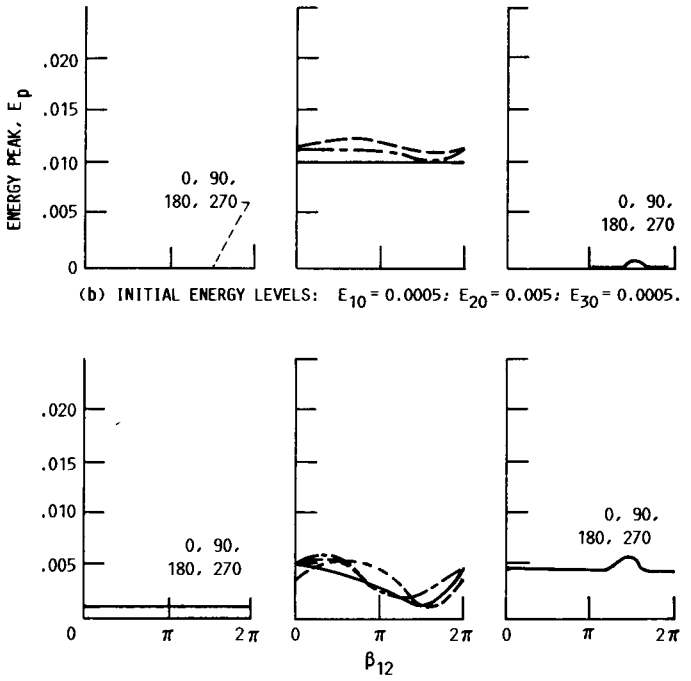

(b) INITIAL ENERGY LEVELS: $E_{10} = 0.0005$; $E_{20} = 0.005$; $E_{30} = 0.0005$.

(c) INITIAL ENERGY LEVELS: $E_{10} = 0.005$; $E_{20} = 0.0005$; $E_{30} = 0.0005$.

FIGURE 25. - EFFECT OF INITIAL PHASE DIFFERENCES, β_{12} AND β_{23}, ON THE PEAK OF EACH FREQUENCY COMPONENT (THREE STROUHAL NUMBERS, S). NONEQUAL INITIAL ENERGY LEVELS.

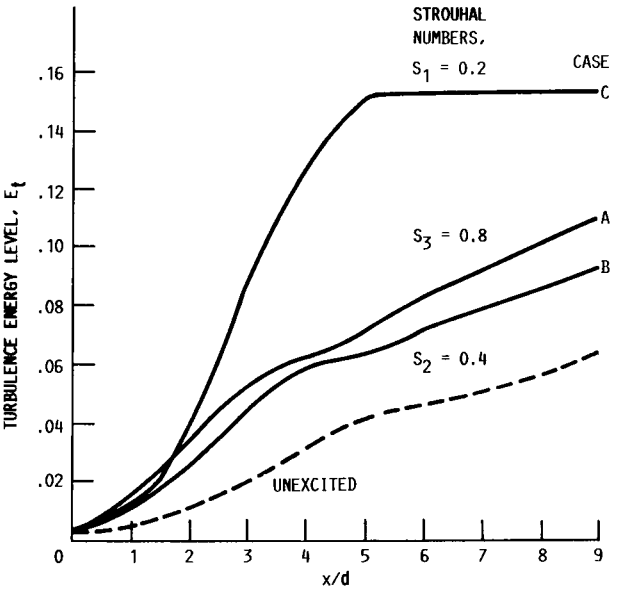

FIGURE 26. - TURBULENCE ENHANCEMENT UNDER VARIABLE RATIOS OF INITIAL ENERGY LEVELS. CASE A: INITIAL PHASE DIFFERENCES, $\beta_{12} = 270^0$; $\beta_{23} = 90^0$; INITIAL ENERGY LEVELS, $E_{10} = 0.0005$; $E_{20} = 0.0005$; $E_{30} = 0.005$. CASE B: $\beta_{12} = 270^0$; $\beta_{23} = 270^0$; $E_{10} = 0.0005$; $E_{20} = 0.005$; $E_{30} = 0.0005$. CASE C: $\beta_{12} = 270^0$; $\beta_{23} = 180^0$; $E_{10} = 0.005$; $E_{20} = 0.0005$; $E_{30} = 0.0005$.

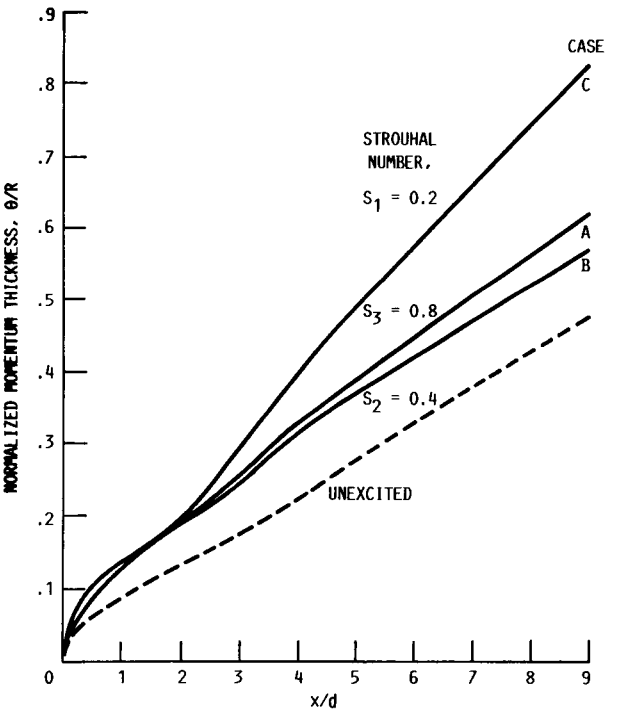

FIGURE 27. - MOMENTUM THICKNESS ENHANCEMENT UNDER VARIABLE RATIOS OF INITIAL ENERGY LEVELS. CASE A: INITIAL PHASE DIFFERENCES, $\beta_{12} = 270^0$; $\beta_{23} = 90^0$; INITIAL ENERGY LEVELS, $E_{10} = 0.0005$; $E_{20} = 0.0005$; $E_{30} = 0.005$. CASE B: $\beta_{12} = 270^0$; $\beta_{23} = 180^0$; $E_{10} = 0.0005$; $E_{20} = 0.005$; $E_{30} = 0.0005$. CASE C: $\beta_{12} = 270^0$; $\beta_{23} = 270^0$; $E_{10} = 0.005$; $E_{20} = 0.0005$; $E_{30} = 0.0005$.

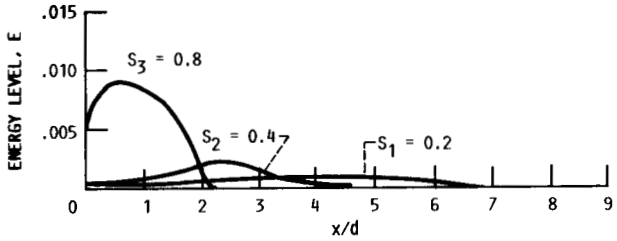

FIGURE 28. - DEVELOPMENT OF THE FREQUENCY COMPONENTS AT NONEQUAL INITIAL ENERGY LEVELS: E_{10} = 0.0005; E_{20} = 0.0005; E_{30} = 0.005. INITIAL PHASE DIFFERENCES: β_{12} = 270^0; β_{23} = 90^0.

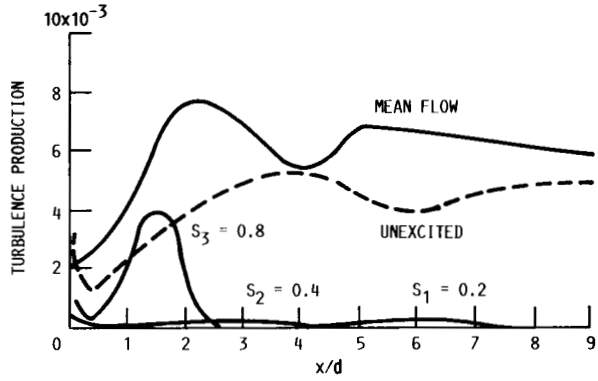

FIGURE 29. - TURBULENCE PRODUCTIONS BY THE MEAN FLOW AND WAVES AT NONEQUAL INITIAL ENERGY LEVELS: E_{10} = 0.0005; E_{20} = 0.0005; E_{30} = 0.005. INITIAL PHASE DIFFERENCES: β_{12} = 270^0; β_{23} = 90^0.

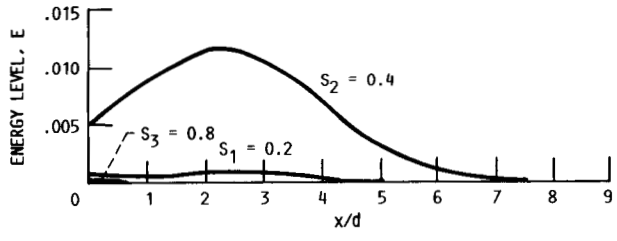

FIGURE 30. - DEVELOPMENT OF THE FREQUENCY COMPONENTS AT NONEQUAL INITIAL ENERGY LEVELS: E_{10} = 0.0005; E_{20} = 0.005; E_{30} = 0.0005. INITIAL PHASE DIFFERENCES: β_{12} = 270^0; β_{23} = 180^0.

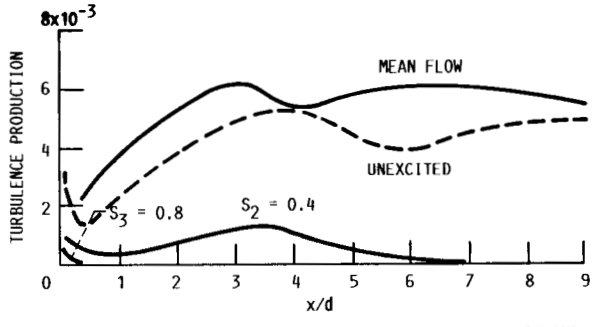

FIGURE 31. - TURBULENCE PRODUCTIONS BY THE MEAN FLOW AND WAVES AT NONEQUAL INITIAL ENERGY LEVELS: E_{10} = 0.0005; E_{20} = 0.005; E_{30} = 0.0005. INITIAL PHASE DIFFERENCES: β_{12} = 270^0; β_{23} = 180^0.

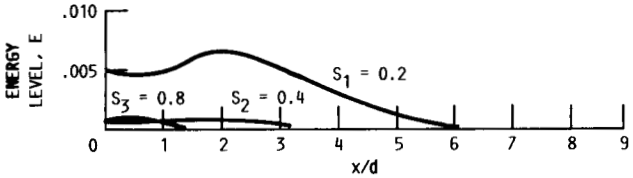

FIGURE 32. - DEVELOPMENT OF THE FREQUENCY COMPONENTS AT NONEQUAL INITIAL ENERGY LEVELS: E_{10} = 0.005; E_{20} = 0.0005; E_{30} = 0.0005. INITIAL PHASE DIFFERENCES: β_{12} = 270^0; β_{23} = 270^0.

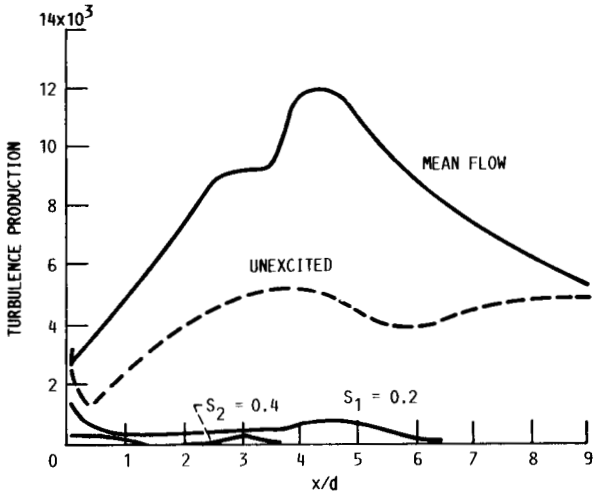

FIGURE 33. - TURBULENCE PRODUCTIONS BY THE MEAN FLOW AND WAVES AT NONEQUAL INITIAL ENERGY LEVELS: E_{10} = 0.005; E_{20} = 0.0005; E_{30} = 0.0005. INITIAL PHASE DIFFERENCES: β_{12} = 270^0; β_{23} = 270^0.

NASA
National Aeronautics and Space Administration

Report Documentation Page

1. Report No.	2. Government Accession No.	3. Recipient's Catalog No.
NASA TM-101985 ICOMP-89-12		

4. Title and Subtitle

Multiwave Interactions in Turbulent Jets

5. Report Date

September 1989

6. Performing Organization Code

7. Author(s)

Reda R. Mankbadi

8. Performing Organization Report No.

E-4685

10. Work Unit No.

505-62-21

9. Performing Organization Name and Address

National Aeronautics and Space Administration
Lewis Research Center
Cleveland, Ohio 44135-3191

11. Contract or Grant No.

13. Type of Report and Period Covered

Technical Memorandum

12. Sponsoring Agency Name and Address

National Aeronautics and Space Administration
Washington, D.C. 20546-0001

14. Sponsoring Agency Code

15. Supplementary Notes

Reda R. Mankbadi, Institute for Computational Mechanics in Propulsion, NASA Lewis Research Center (work funded under Space Act Agreement C99066G). Space Act Monitor, Louis A. Povinelli.

16. Abstract

Nonlinear wave-wave interactions in turbulent jets were investigated based on the integrated energy of each scale of motion in a cross section of the jet. The analysis indicates that two frequency components in the axisymmetric mode can interact with other background frequencies in the axisymmetric mode, thereby amplifying an enormous number of other frequencies. Two frequency components in a single helical mode cannot, by themselves, amplify other frequency components. But combinations of frequency components of helical and axisymmetric modes can amplify other frequencies in other helical modes. The present computations produce several features consistent with experimental observations such as (1) dependency of the interactions on the initial phase differences, (2) enhancement of the momentum thickness under multifrequency forcing, and (3) the increase in background turbulence under forcing. In a multifrequency-excited jet, mixing enhancement was found to be a result of the turbulence enhancement rather than simply the amplification of forced wave components. The excitation waves pump energy from the mean flow to the turbulence, thus enhancing the latter. The high-frequency waves enhance the turbulence close to the jet exit, but, the low-frequency waves are most effective further downstream.

17. Key Words (Suggested by Author(s))	18. Distribution Statement
Shear layers; Round jets; Nonlinear stability; Transition; Excited jets	Unclassified – Unlimited Subject Category 34

19. Security Classif. (of this report)	20. Security Classif. (of this page)	21. No of pages	22. Price*
Unclassified	Unclassified	46	A03

NASA FORM 1626 OCT 86

*For sale by the National Technical Information Service, Springfield, Virginia 22161